64 $(CH_3NHCH_2COOH)_3 \cdot CaCl_2$ family

64A Pure compounds

No. 64A-1 $(CH_3NHCH_2COOH)_3 \cdot CaCl_2$, Tris-sarcosine calcium chloride (TSCC)

(M = 378.27)

1a Ferroelectric activity in $(CH_3NHCH_2COOH)_3 \cdot CaCl_2$ was discovered by Pepinsky et al. in 1962. 62Pep

b

phase	II	I	[a]) 65Mak
state	F	P	[b]) 84Mis
crystal system	orthorhombic	orthorhombic	
space group	$Pn2_1a - C_{2v}^{9}$ [b])	$Pnma - D_{2h}^{16}$ [a])	
Θ [K]	127		

$P_s \parallel [010]$. 65Mak
$\rho = 1.533 \cdot 10^3$ kg m^{-3} at RT. 65Mak
$\rho = 1.55 \cdot 10^3$ kg m^{-3} at 118(1) K. 84Mis
Transparent, colorless. 65Mak

2a Crystal growth: evaporation or cooling method from aqueous solution. 65Mak

3a Unit cell parameters: a = 9.156(10) Å, b = 17.460(5) Å, c = 10.265(5) Å at RT. 65Mak
Unit cell parameters: a = 9.122(4) Å, b = 17.408(4) Å, c = 10.228(8) Å at 118(1) K. 84Mis

b Z = 4 in phases I and II. 65Mak
Crystal structure of phase I: Table 64A-1-001, Table 64A-1-002, Table 64A-1-003; Fig. 64A-1-001, Fig. 64A-1-002, Fig. 64A-1-003, Fig. 64A-1-004, Fig. 64A-1-005.
Crystal structure of phase II: Table 64A-1-004, Table 64A-1-005, Table 64A-1-006; Fig. 64A-1-006, Fig. 64A-1-007, Fig. 64A-1-008.
Temperature dependence of temperature parameters: Fig. 64A-1-009, Fig. 64A-1-010.

4 Lattice distortion: Fig. 64A-1-011.

5a Dielectric constants: Fig. 64A-1-012, Fig. 64A-1-013, Fig. 64A-1-014, Fig. 64A-1-015, Fig. 64A-1-016, Fig. 64A-1-017, Fig. 64A-1-018, Fig. 64A-1-019, Fig. 64A-1-020, Fig. 64A-1-021; see also 86Paw
$\Theta_f - \Theta_p$ = 0.4(1) K, C = 59(3) K. 65Mak
Phase diagram in regard to p: Fig. 64A-1-022.
Curie-Weiss constant including the data of $(CH_3NHCH_2COOH)_3 \cdot Ca(Cl_{1-x}I_x)_2$: Table 64A-1-007; see also Fig. 64A-2-003 in No. 64A-2.

b Values of ξ and ζ including the data of $(CH_3NHCH_2COOH)_3 \cdot Ca(Cl_{1-x}I_x)_2$: Table 64A-1-007.

c Spontaneous polarization and coercive field: Fig. 64A-1-023, Fig. 64A-1-024, Fig. 64A-1-025, Fig. 64A-1-026; see also Fig. 64A-1-058 in subsection 13b.

6a Heat capacity: Fig. 64A-1-027, Fig. 64A-1-028.
Transition heat ΔQ_m and transition entropy ΔS_m:
ΔQ_m = 446(80) J mol^{-1}, ΔS_m = 4.26(80) J K^{-1} mol^{-1}. 79Mat

b Thermal conductivity: Fig. 64A-1-029.

8a	Elastic stiffness: Fig. 64A-1-030. See also subsection 10b.	
9a	Birefringence: Fig. 64A-1-031. Far-infrared spectra: Fig. 64A-1-032.	
b	Electrooptic effect: Fig. 64A-1-033.	
c	Piezoelectric effect: Fig. 64A-1-031.	
10a	Pressure dependence of Raman spectra: see Raman spectra of a soft mode: Fig. 64A-1-034, Fig. 64A-1-035, Fig. 64A-1-036.	85Rot
b	Brillouin scattering: Fig. 64A-1-037, Fig. 64A-1-038, Fig. 64A-1-039, Fig. 64A-1-040, Fig. 64A-1-041, Fig. 64A-1-042, Fig. 64A-1-043, Fig. 64A-1-044, Fig. 64A-1-045, Fig. 64A-1-046.	
13a	NMR: Table 64A-1-008; Fig. 64A-1-047, Fig. 64A-1-048, Fig. 64A-1-049, Fig. 64A-1-050, Fig. 64A-1-051, Fig. 64A-1-052.	
b	ESR and ENDOR: Table 64A-1-009, Table 64A-1-010, Table 64A-1-011, Table 64A-1-012, Table 64A-1-013; Fig. 64A-1-053, Fig. 64A-1-054, Fig. 64A-1-055, Fig. 64A-1-056, Fig. 64A-1-057, Fig. 64A-1-058, Fig. 64A-1-059.	
	Parameters of spin Hamiltonian of Mn^{2+} at RT: $g = 2.005(1)$, $D = 192(1) \cdot 10^{-2}$ m^{-1}, $E = -14.2(5) \cdot 10^{-2}$ m^{-1}, $A = -88(1) \cdot 10^{-2}$ m^{-1}, $a = 6(3) \cdot 10^{-2}$ m^{-1}.	72Bar
	For ESR of Mn^{2+}, see also	75Win
	For the correlation time determined from Mn^{2+} ESR: see	81Vol

Table 64A-1-001. $(CH_3NHCH_2COOH)_3 \cdot CaCl_2$. Crystal structure of phase I [72Ash]. Fractional coordinates and temperature parameters. The temperature parameters are defined by Eq. (a) in Introduction. For molecules 1, 2 see also Fig. 64A-1-003.

	x	y	z	B_{11}	B_{22}	B_{33}	B_{12}	B_{13}	B_{23}
	10^{-4}			10^{-4}					
Ca	386(2)	2500(0)	2249(1)	42(2)	6(1)	16(2)	0(0)	2(3)	0(0)
Cl	4912(2)	833(1)	7148(1)	96(2)	15(1)	47(2)	10(2)	0(3)	–2(1)
Molecule 1									
O(11)	1720(8)	2500(0)	4142(6)	120(10)	38(3)	40(6)	0(0)	–84(14)	0(0)
O(12)	4070(7)	2500(0)	4718(5)	76(8)	27(2)	34(6)	0(0)	44(11)	0(0)
N(11)	3511(8)	2500(0)	7265(6)	84(10)	15(2)	5(6)	0(0)	7(13)	0(0)
C(11)	2747(10)	2500(0)	4942(8)	120(14)	8(3)	24(8)	0(0)	–11(18)	0(0)
C(12)	2228(9)	2500(0)	6378(8)	67(11)	20(3)	29(8)	0(0)	–18(16)	0(0)
C(13)	3003(12)	2500(0)	8659(9)	141(16)	31(4)	30(9)	0(0)	11(20)	0(0)
Molecule 2									
O(21)	6588(5)	1447(2)	3713(4)	103(6)	18(2)	74(5)	36(5)	0(10)	25(5)
O(22)	8936(6)	1601(3)	3240(5)	145(8)	23(2)	77(5)	–55(6)	54(11)	21(5)
N(21)	7000(6)	114(3)	4937(5)	91(7)	10(2)	42(5)	–1(6)	15(10)	13(5)
C(21)	7899(7)	1263(3)	3732(5)	91(8)	10(2)	25(5)	–12(7)	8(11)	–4(5)
C(22)	8309(7)	532(3)	4464(6)	55(7)	13(2)	42(6)	9(6)	16(11)	10(6)
C(23)	7380(9)	–576(4)	5733(7)	166(12)	14(2)	100(9)	–12(9)	–17(18)	48(8)

Table 64A-1-002. $(CH_3NHCH_2COOH)_3 \cdot CaCl_2$. Crystal structure of phase I [72Ash]. Fractional coordinates of hydrogen atoms.

Atom	*x*	*y*	*z*	Bonded to
H(11)	0.165	0.193	0.653	C(12)
H(13)	0.410	0.202	0.712	N(11)
H(15)	0.373	0.250	0.910	C(13)
H(17)	0.248	0.193	0.858	C(13)
H(21)	0.878	0.014	0.384	C(22)
H(22)	0.894	0.069	0.530	C(22)
H(23)	0.648	–0.011	0.420	N(21)
H(24)	0.655	0.037	0.546	N(22)
H(25)	0.634	–0.082	0.595	C(23)
H(26)	0.805	–0.025	0.660	C(23)
H(27)	0.808	–0.093	0.521	C(23)

Table 64A-1-003. $(CH_3NHCH_2COOH)_3 \cdot CaCl_2$. Crystal structure of phase I [72Ash]. Hydrogen bonds I, II, III (see Fig. 64A-1-001, Fig. 64A-1-002). C(M): carbon atom of the methyl group. C(α): carbon atom of the carboxyl group of sarcosine molecule.

H-bond	N...Cl	H...CL	∢ NHCl	∢C(α)NCl	∢C(M)NCl
I	3.182 Å	2.20 Å	164°	107.2°	99.2°
II	3.222 Å	2.43 Å	165°	121.2°	93.9°
III	3.222 Å	2.27 Å	166°	118.3°	94.3°

N–Cl–N angle between I and II: 128.5°
I and III: 106.0°
II and III: 69.8°

Table 64A-1-004. $(CH_3NHCH_2COOH)_3 \cdot CaCl_2$. Crystal structure [84Mis]. T = 118 K. Fractional coordinates and isotropic temperature parameters. For molecules 1, 2, 3 see also Fig. 64A-1-006, Fig. 64A-1-007. $\overline{u^2} = B/(8\pi^2)$, where B is defined in Eq. (e) in Introduction.

	x	y	z	$\overline{u^2}$ [10^{-2} Å^2]
Ca	0.03820(2)	0.25	0.22421(2)	0.710(3)
Cl(1)	0.48664(8)	0.08389(4)	0.71533(7)	1.41(1)
Cl(2)	0.49575(5)	0.41780(5)	0.71399(6)	1.39(1)
Molecule 1				
O(11)	0.1681(1)	0.2522(2)	0.4165(1)	1.91(2)
O(12)	0.4059(1)	0.2490(2)	0.4744(1)	1.46(2)
N(1)	0.3514(1)	0.2519(2)	0.7299(1)	1.07(2)
C(11)	0.2716(1)	0.2510(2)	0.4970(1)	1.06(2)
C(12)	0.2239(1)	0.2517(2)	0.6400(1)	1.11(2)
C(13)	0.3054(2)	0.2522(2)	0.8694(1)	1.90(3)
Molecule 2				
O(21)	0.6656(2)	0.1475(1)	0.3746(2)	1.55(3)
O(22)	0.9037(2)	0.1540(1)	0.3206(2)	1.92(4)
N(2)	0.6944(2)	0.0111(1)	0.4952(2)	1.19(3)
C(21)	0.7954(2)	0.1244(1)	0.3739(2)	1.04(4)
C(22)	0.8295(2)	0.0507(1)	0.4477(3)	1.09(4)
C(23)	0.7275(3)	–0.0567(2)	0.5763(3)	2.09(5)
Molecule 3				
O(31)	0.6468(2)	0.3613(1)	0.3718(2)	1.89(4)
O(32)	0.8809(2)	0.3345(1)	0.3239(2)	2.37(4)
N(3)	0.7076(2)	0.4916(1)	0.4947(2)	1.11(3)
C(31)	0.7819(2)	0.3744(1)	0.3740(2)	1.14(4)
C(32)	0.8328(2)	0.4459(1)	0.4459(2)	1.11(3)
C(33)	0.7557(3)	0.5608(2)	0.5713(3)	2.28(6)

Table 64A-1-005. $(CH_3NHCH_2COOH)_3 \cdot CaCl_2$. Crystal structure [84Mis]. Positional differences between the ferroelectric structure (T = 118 K) and the paraelectric structure (T = RT).

	$a\Delta x$	$b\Delta y$	$c\Delta z$
	[Å]		
Ca	–0.004(2)	0.0	–0.007(1)
Cl(1)	–0.042(2)	0.010(2)	0.005(1)
Cl(2)	0.042(2)	0.019(2)	–0.008(1)
Molecule 1			
O(11)	–0.035(7)	0.039(3)	0.024(6)
O(12)	–0.010(7)	–0.018(3)	0.026(5)
N(1)	0.003(7)	0.032(3)	0.035(6)
C(11)	–0.028(9)	0.017(3)	0.029(8)
C(12)	0.010(8)	0.030(3)	0.022(8)
C(13)	0.047(11)	0.038(4)	0.036(9)
Molecule 2			
O(21)	0.062(5)	0.049(4)	0.034(5)
O(22)	0.092(6)	–0.106(6)	–0.035(6)
N(2)	–0.051(6)	–0.006(6)	0.015(6)
C(21)	0.050(7)	–0.033(6)	0.007(6)
C(22)	–0.012(7)	–0.044(6)	0.013(7)
C(23)	–0.096(9)	0.016(8)	0.030(8)
Molecule 3			
O(31)	–0.100(5)	0.104(4)	0.005(5)
O(32)	–0.116(6)	–0.093(6)	–0.001(6)
N(3)	0.069(6)	0.052(6)	0.010(6)
C(31)	–0.073(7)	0.013(6)	0.008(6)
C(32)	0.017(7)	–0.015(6)	–0.005(7)
C(33)	0.162(9)	0.056(8)	–0.020(8)

Table 64A-1-006. $(CH_3NHCH_2COOH)_3 \cdot CaCl_2$. Crystal structure [84Mis]. T = 118 K. Dimensions of the N–H ··· Cl hydrogen bonds and those of the neighbors. See Fig. 64A-1-006 about the notation. C(M): carbon atom of the methyl group.

H-bond	N...Cl	H...CL	∢ NHCl	∢CNCl	∢C(M)NCl	N–Cl–N angle	
	[Å]	[Å]	[°]	[°]	[°]	between	[°]
I	3.178(3)	2.27(5)	161(5)	105.9(2)	99.1(2)	I and II	128.80(5)
I'	3.178(3)	2.42(5)	160(5)	107.2(2)	99.4(2)	I' and II'	130.20(5)
II	3.204(2)	2.31(6)	156(5)	122.3(1)	92.4(2)	I and III	106.10(5)
II'	3.227(2)	2.39(6)	164(5)	118.9(1)	97.6(2)	I' and III'	105.73(5)
III	3.215(2)	2.24(5)	158(4)	118.0(1)	96.2(1)	II and III	70.05(6)
III'	3.198(2)	2.39(5)	161(5)	117.7(2)	94.6(2)	II' and III'	69.98(6)

Table 64A-1-007. $(CH_3NHCH_2COOH)_3 \cdot Ca(Cl_{1-x}I_x)_2$. C, Θ_p, ξ, ζ vs. x [84Fuj]. $\kappa_b - \kappa_\infty = C/(T - \Theta_p)$, $E = (1/\chi_p)\, P + \xi P^3 + \zeta P^5$.

x	0.00	0.09	0.18	0.25
Θ_p [°C]	–146	–170	–193	–223
C [K]	35.0	37.0	43.5	29.0
ξ [10^{15} Vm^5 C^{-3}]	7.2	40.3	258	1110
ζ [10^{21} Vm^9 C^{-5}]	1.2	27.1	503	2760

Table 64A-1-008. $(CH_3NHCH_2COOH)_3 \cdot CaCl_2$. Nuclear quadrupole resonance frequencies, e^2qQ/h and η of ^{14}N, ^{35}Cl, and ^{37}Cl [75Bli].

T [K]	Nucleus	Resonance frequencies [kHz]			e^2qQ/h [kHz]	η
292	N(1)	1040,	520,	520	1040	1
	N(2), N(3)	940,	470,	470	940	1
	^{35}Cl		2160	...	...	...
	^{37}Cl		1710		...	...
77	N	980,	530,	450	1010	0.89

Table 64A-1-009. $(CH_3NHCH_2COOH)_3 \cdot CaCl_2:VO^{2+}$. Spin Hamiltonian parameters [78Sat].

Spectrum	$g_\parallel$	$g_\perp$	A [10^2 m^{-1}]	B [10^2 m^{-1}]
I	1.911(2)	1.987(2)	174(2)	79(2)
II	1.930(2)	1.991(2)	178(2)	72(2)

Table 64A-1-010. $(CH_3NHCH_2COOH)_3 \cdot CaCl_2:Mn^{2+}$, $(CH_3NHCH_2COOH)_3 \cdot CaBr_2:Mn^{2+}$. Spin Hamiltonian parameters of Mn^{2+} [75Nav]. A, D, E and a are in [$\cdot 10^{-2}$ m^{-1}]. For spin lattice relaxation time, see [78Bru].

	g	A	D	E	a
$(CH_3NHCH_2COOH)_3 \cdot CaCl_2$	2.005	–88	192	14	6
$(CH_3NHCH_2COOH)_3 \cdot CaBr_2$	2.005	–84	151	21	5

Table 64A-1-011. $(CH_3NHCH_2COOH)_3 \cdot CaCl_2:VO^{2+}$. ^{51}V HFS tensor for VO^{2+} [83Fuj]. T = 22.5 °C. Spectra I', II' are satellites of spectra I and II, respectively. Double signs for b and c components should be combined in four ways for the magnetically equivalent directions. Spectrum II*: an additional spectrum to the spectrum II appeared after heating.

Spectrum	Principal value [10^2 Am^{-1}]	Direction cosine
II	147.2	(0.6224, ± 0.6731, ± 0.3962)
	55.7	(0.3294, ± 0.2330, ∓ 0.9150)
	54.5	(0.7097, ∓ 0.7008, ± 0.0721)
II'	145.2	(0.6252, ± 0.6585, ± 0.4190)
	60.6	(–0.7197, ± 0.6941, ∓ 0.0171)
	54.4	(–0.3028, ∓ 0.2901, ± 0.9078)
II*	147.4	(0.7202, ± 0.6011, ± 0.3465)
	56.0	(0.1300, ± 0.3737, ∓ 0.9184)
	54.0	(–0.6816, ± 0.7063, ± 0.1913)
I	151.2	(0.6217, 0, ± 0.7833)
	59.4	(0, ± 1, 0)
	54.2	(–0.7833, 0, ± 0.6216)
I'	151.4	(0.6177, 0, ± 0.7864)
	59.4	(0, ± 1, 0)
	55.7	(–0.7864, 0, ± 0.6177)

Table 64A-1-012. $(CH_3NHCH_2COOH)_3 \cdot CaCl_2:Mn^{2+}$. Principal values of HFS tensors of the six ^{13}C nuclei by Mn^{2+} ENDOR [83Met].

		Principal value [kHz]		Direction cosine
C(11)	A_{aniso}^{exp}	A_1	1200	(0.7657, 0.0191, –0.6429)
		A_2	–570	
		A_3	–630	
		A_{iso}	750	
C(41)		A_1	1150	(–0.6282, –0.0103, 0.7780)
		A_2	–640	
		A_3	–510	
		A_{iso}	1550	
C(21)		A_1	1240	(0.7361, –0.6247, 0.2606)
		A_2	–720	
		A_3	–520	
		A_{iso}	610	
C(61)		A_1	1170	(0.7415, 0.6290, 0.2336)
		A_2	–570	
		A_3	–600	
		A_{iso}	900	
C(31)		A_1	1160	(0.6784, 0.6020, 0.4211)
		A_2	–630	
		A_3	–530	
		A_{iso}	1880	
C(51)		A_1	1150	(0.6788, –0.5653, 0.4687)
		A_2	–650	
		A_3	–500	
		A_{iso}	1350	

Table 64A-1-013. $(CH_3NHCH_2COOH)_3 \cdot CaCl_2:Mn^{2+}$. Spin Hamiltonian parameters for Mn^{2+} [83Kuc].

	TSCC:Mn^{2+}
g	2.001(1)
A [10^6 m^{-1}]	–90.5(5)
D [10^6 m^{-1}]	191.5(5)
E [10^6 m^{-1}]	13.3(5)

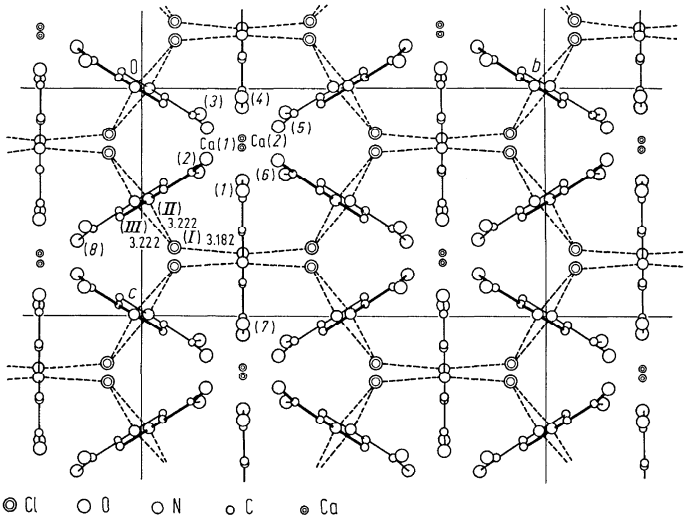

Fig. 64A-1-001. $(CH_3NHCH_2COOH)_3 \cdot CaCl_2$. Crystal structure of phase I [72Ash]. Projection on (100). The sarcosine molecules are disignated by Arabic numerals, the hydrogen bonds (dashed lines) by Roman numerals, whose notation is the same as that in Fig. 64A-1-002. Distances in [Å].

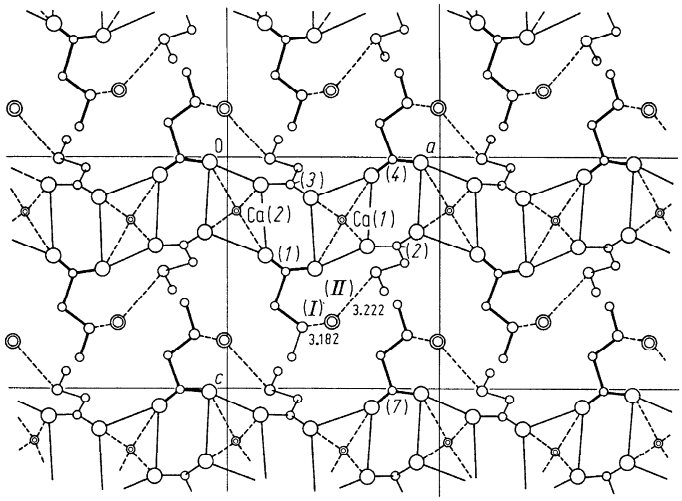

Fig. 64A-1-002. $(CH_3NHCH_2COOH)_3 \cdot CaCl_2$. Crystal structure of phase I [72Ash]. Projection on (010). See notation and caption of Fig. 64A-1-001.

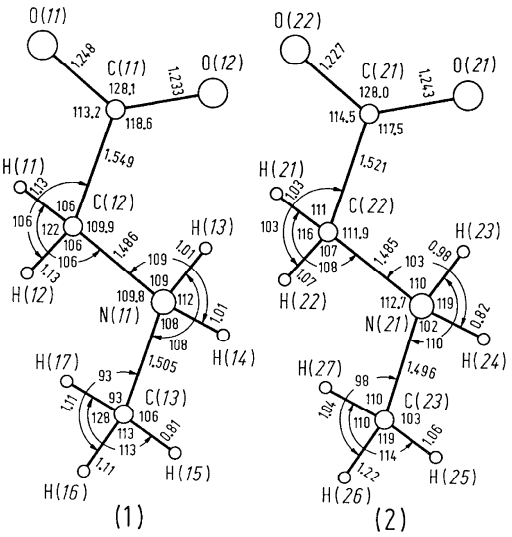

Fig. 64A-1-003. $(CH_3NHCH_2COOH)_3 \cdot CaCl_2$. Crystal structure of phase I [72Ash]. Interatomic distances [Å] and bond angles [°] in sarcosine molecules. The molecule on the left hand side, (1), is in the mirror plane, while the one on the right, (2), is in the general position.

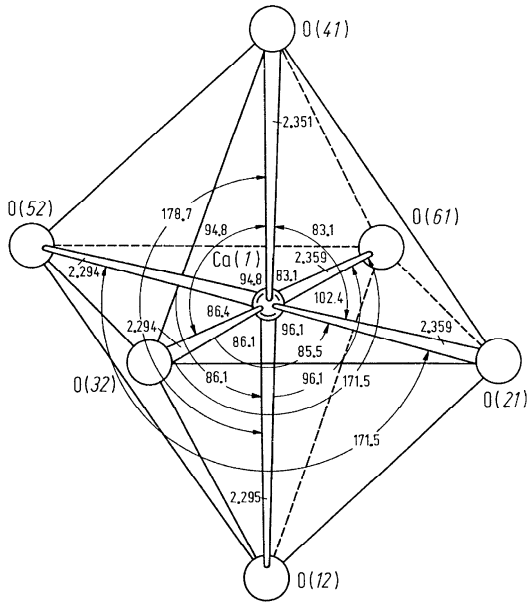

Fig. 64A-1-004. $(CH_3NHCH_2COOH)_3 \cdot CaCl_2$. Crystal structure of phase I [72Ash]. Geometry of the octahedron around the Ca ion. Interatomic distances [Å] and bond angles [°].

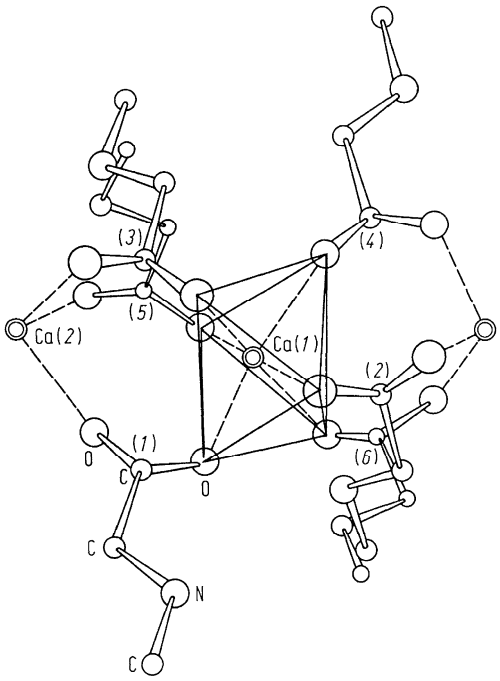

Fig. 64A-1-005. $(CH_3NHCH_2COOH)_3 \cdot CaCl_2$. Crystal structure of phase I [72Ash]. A sketch of the neighbours of the Ca ion. The molecules (1) and (4) and the Ca ion are in the mirror plane, while others are in general position. The molecule (2) is the mirror image of the molecule (6), and (3) is the mirror image of (5).

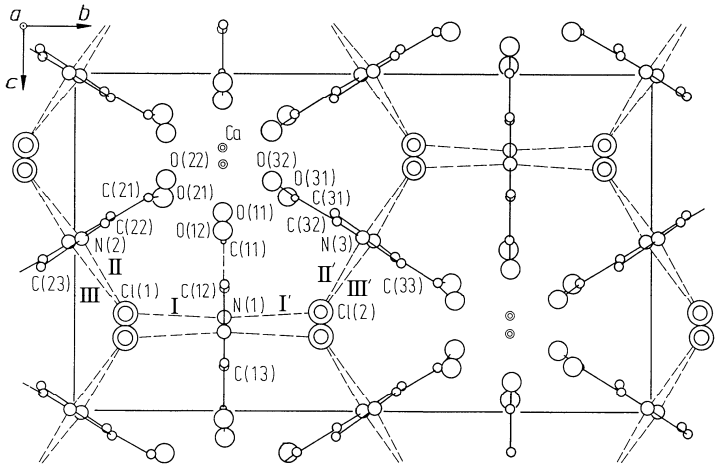

Fig. 64A-1-006. $(CH_3NHCH_2COOH)_3 \cdot CaCl_2$. Crystal structure [84Mis]. $T = 118$ K. Projection along *a*.

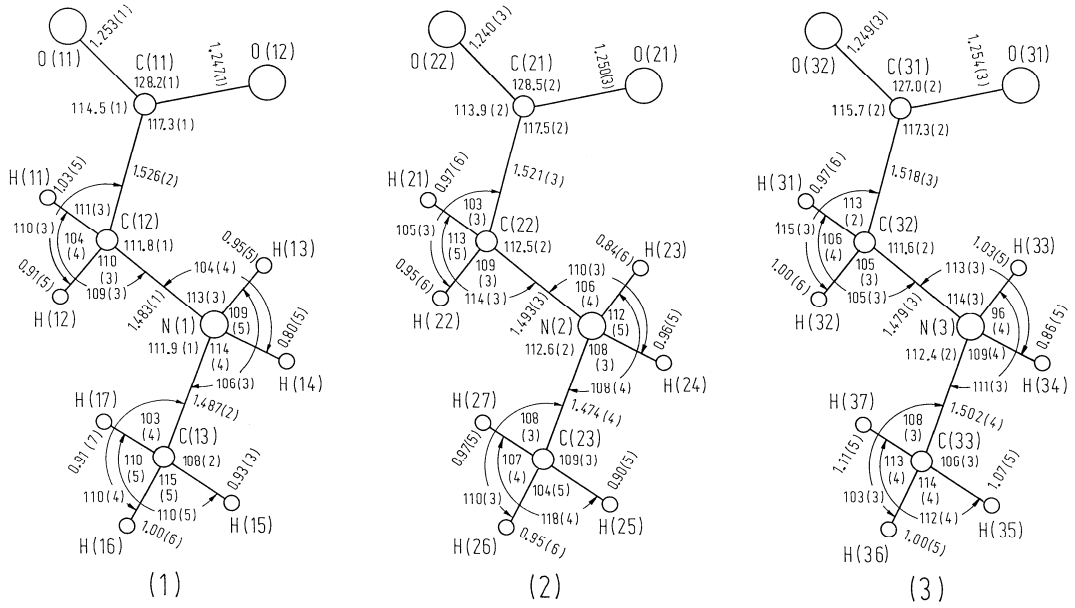

Fig. 64A-1-007. $(CH_3NHCH_2COOH)_3 \cdot CaCl_2$. Crystal structure [84Mis]. T = 118 K. Bond distances [Å] and angles [°] in the three independent sarcosine molecules.

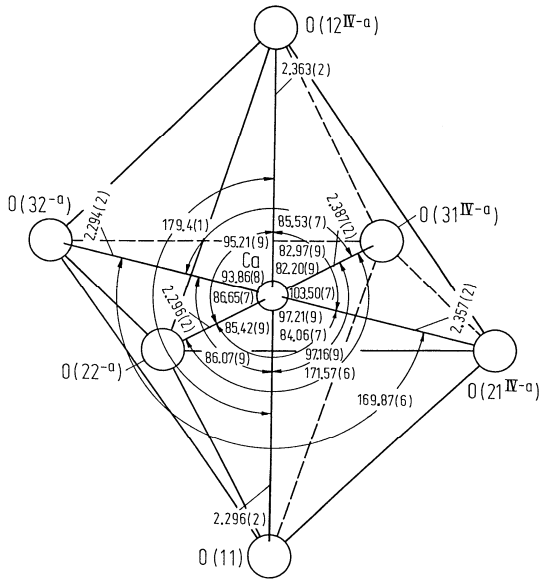

Fig. 64A-1-008. $(CH_3NHCH_2COOH)_3 \cdot CaCl_2$. Crystal structure [84Mis]. T = 118 K. Interatomic distances [Å] and angles [°] of the oxygen octahedral arrangement around Ca. The superscript IV means a symmetry operator from x, y, z to $x + 1/2$, y, $z - 1/2$, while the superscript –a means a translational operator from x, y, z to $x - 1$, y, z.

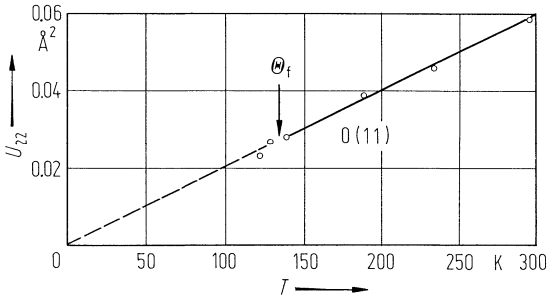

Fig. 64A-1-009. $(CH_3NHCH_2COOH)_3 \cdot CaCl_2$. U_{22} of O(11) vs. T [85Nak]. U_{22}: temperature parameter defined by Eq. (d) in Introduction.

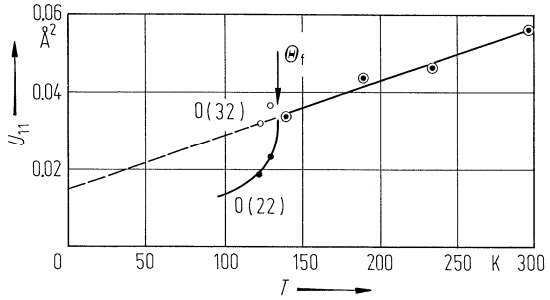

Fig. 64A-1-010. $(CH_3NHCH_2COOH)_3 \cdot CaCl_2$. U_{11} of O(32) and O(22) vs. T [85Nak]. U_{11}: temperature parameter defined by Eq. (d) in Introduction.

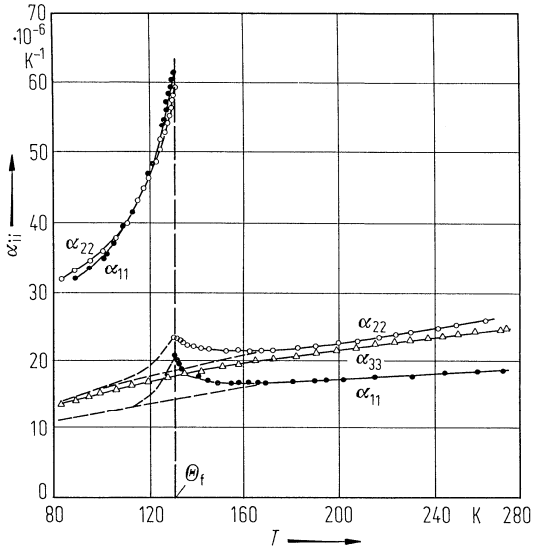

Fig. 64A-1-011. $(CH_3NHCH_2COOH)_3 \cdot CaCl_2$. α_{ii} vs. T [81Sor]. α_{ii}: linear thermal expansion coefficients.

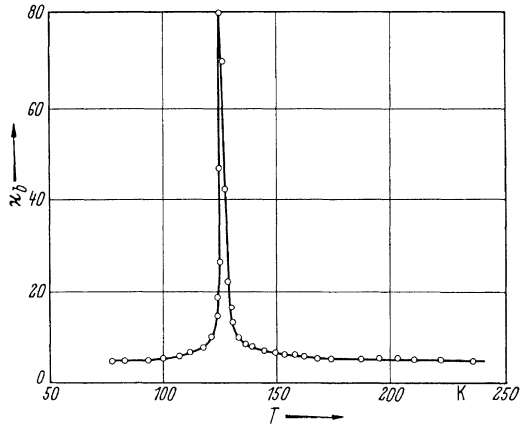

Fig. 64A-1-012. $(CH_3NHCH_2COOH)_3 \cdot CaCl_2$. κ_b vs. T [65Mak]. f = 10 kHz.

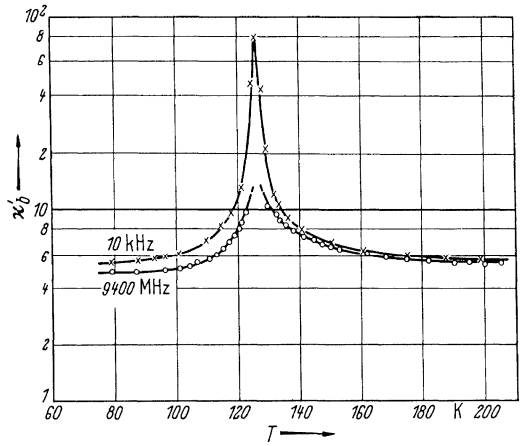

Fig. 64A-1-013. $(CH_3NHCH_2COOH)_3 \cdot CaCl_2$. κ'_b vs. T [65Mak]. Parameter: f.

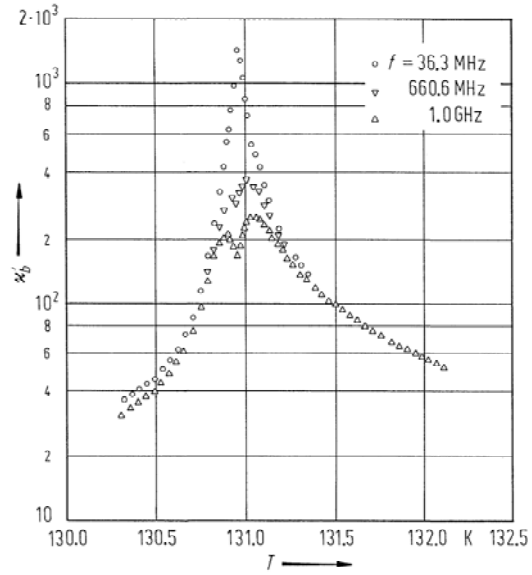

Fig. 64A-1-014. $(CH_3NHCH_2COOH)_3 \cdot CaCl_2$. κ'_b vs. T [83Deg]. Parameter: f.

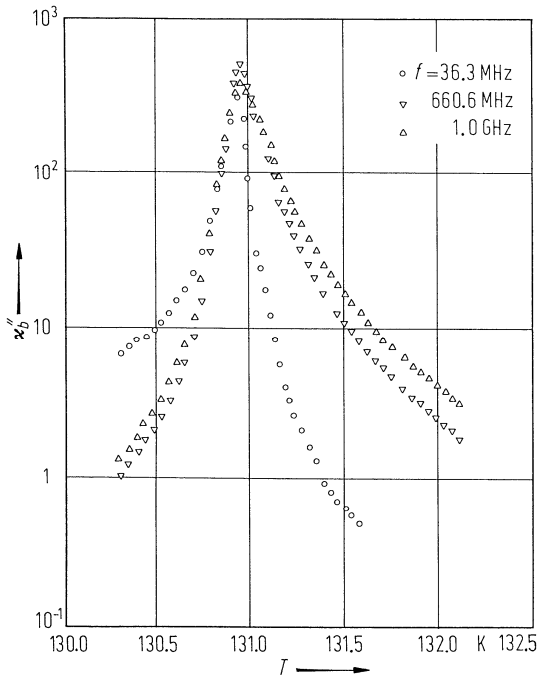

Fig. 64A-1-015. $(CH_3NHCH_2COOH)_3 \cdot CaCl_2$. κ''_b vs. T [83Deg]. Parameter: *f*.

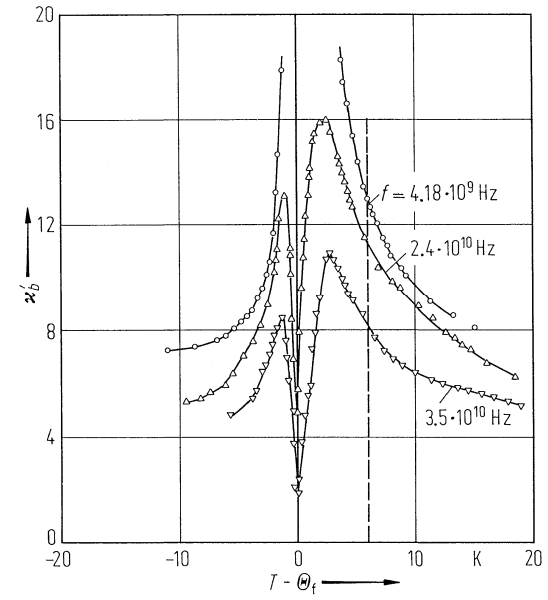

Fig. 64A-1-016. $(CH_3NHCH_2COOH)_3 \cdot CaCl_2$. κ'_b vs. $T - \Theta_f$ [85Saw]. Parameter: *f*.

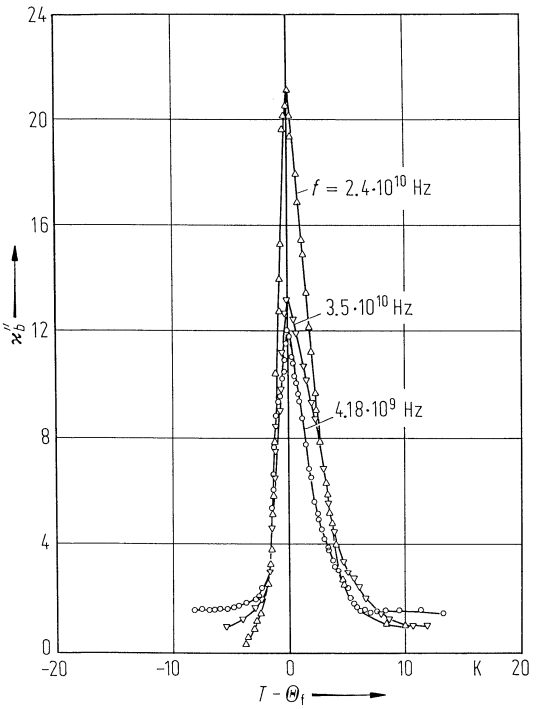

Fig. 64A-1-017. $(CH_3NHCH_2COOH)_3 \cdot CaCl_2$. κ_b'' vs. $T - \Theta_f$ [85Saw]. Parameter: f.

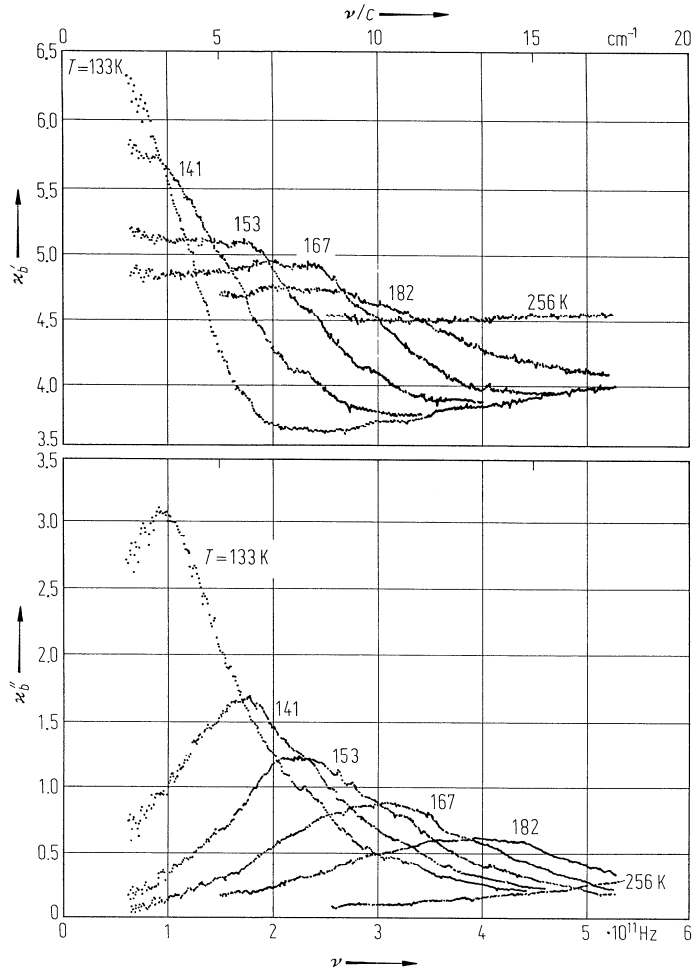

Fig. 64A-1-018. $(CH_3NHCH_2COOH)_3 \cdot CaCl_2$. κ_b', κ_b'' vs. ν [83Koz]. Parameter: T.

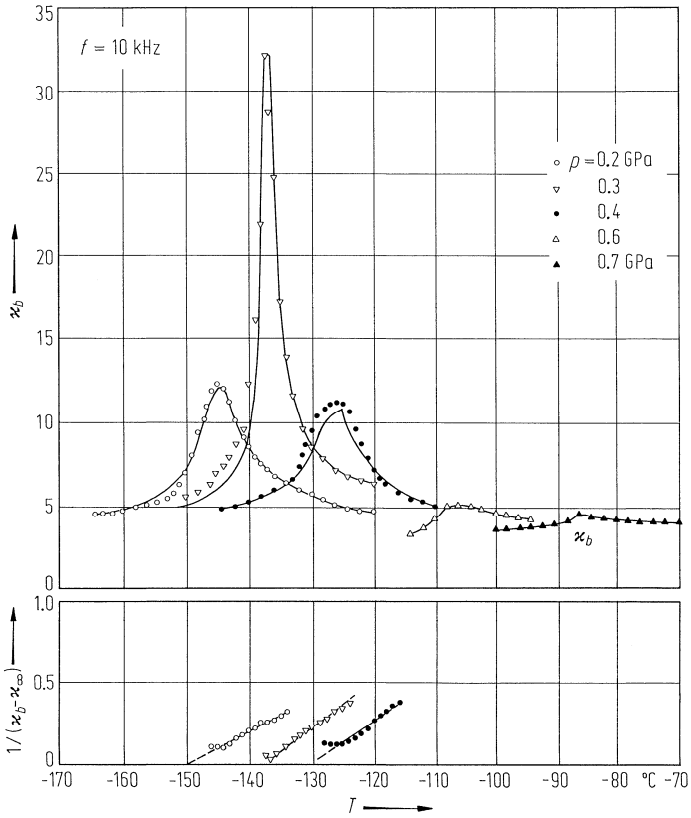

Fig. 64A-1-019. $(CH_3NHCH_2COOH)_3 \cdot Ca(Cl_{0.91}I_{0.09})_2$. $\varkappa_b$, $1/(\varkappa_b - \varkappa_\infty)$ vs. T [84Fuj]. Parameter: p. $\varkappa_\infty = 4.0$.

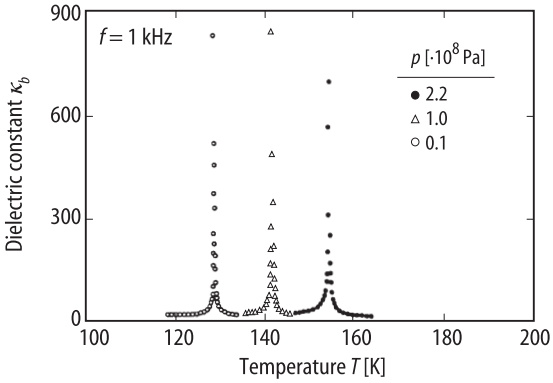

Fig. 64A-1-020. $(CH_3NHCH_2COOH)_3 \cdot CaCl_2$. κ_b vs. T [92Hik]. Parameter: p.

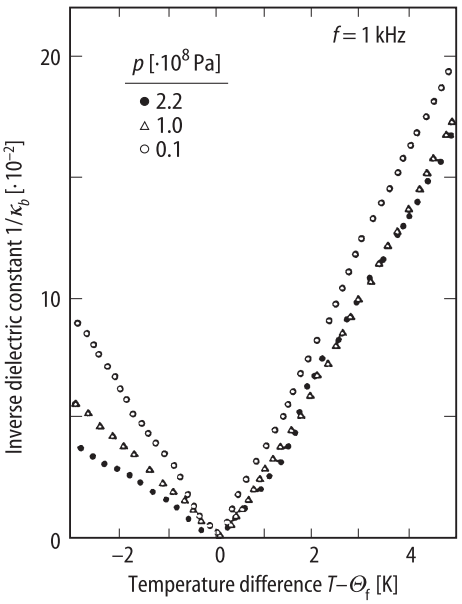

Fig. 64A-1-021. $(CH_3NHCH_2COOH)_3 \cdot CaCl_2$. $1/\kappa_b$ vs. $T - \Theta_f$ [92Hik]. Parameter: p.

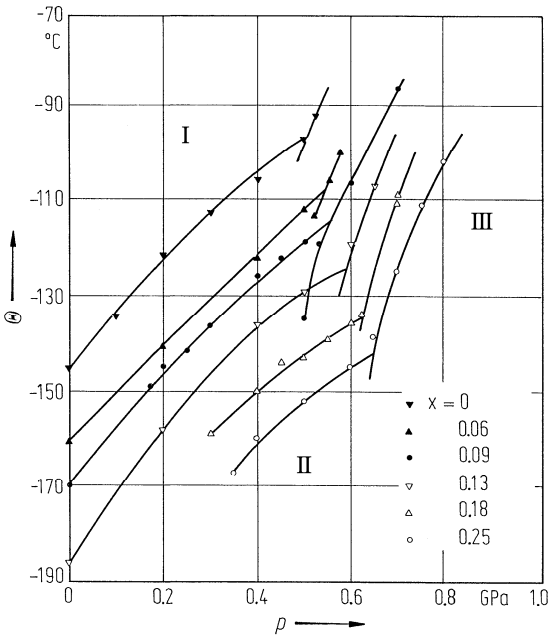

Fig. 64A-1-022. $(CH_3NHCH_2COOH)_3 \cdot Ca(Cl_{1-x}I_x)_2$. Θ vs. p for various x [84Fuj].

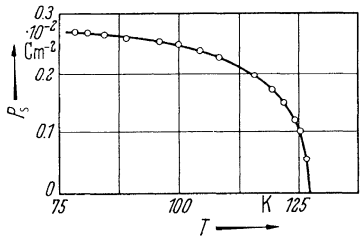

Fig. 64A-1-023. $(CH_3NHCH_2COOH)_3 \cdot CaCl_2$. P_s vs. T [65Mak].

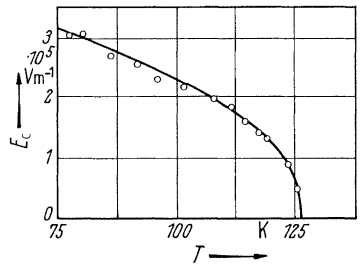

Fig. 64A-1-024. $(CH_3NHCH_2COOH)_3 \cdot CaCl_2$. E_c vs. T [65Mak].

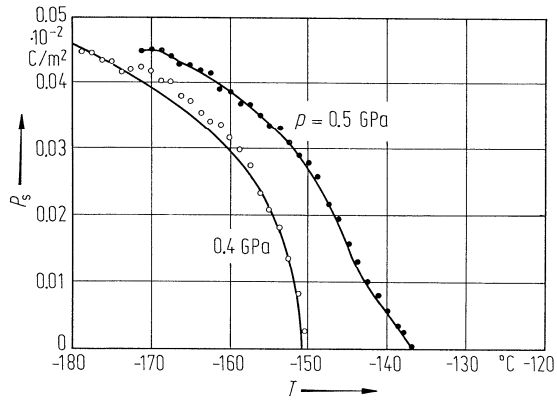

Fig. 64A-1-025. $(CH_3NHCH_2COOH)_3 \cdot Ca(Cl_{0.82}I_{0.18})_2$. P_s vs. T [84Fuj]. Parameter: p.

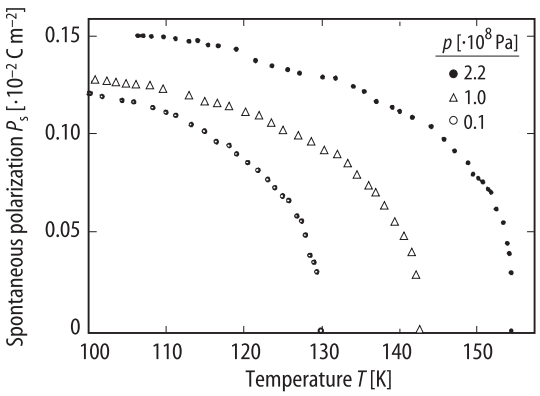

Fig. 64A-1-026. $(CH_3NHCH_2COOH)_3 \cdot CaCl_2$. P_s vs. T [92Hik]. Parameter: p.

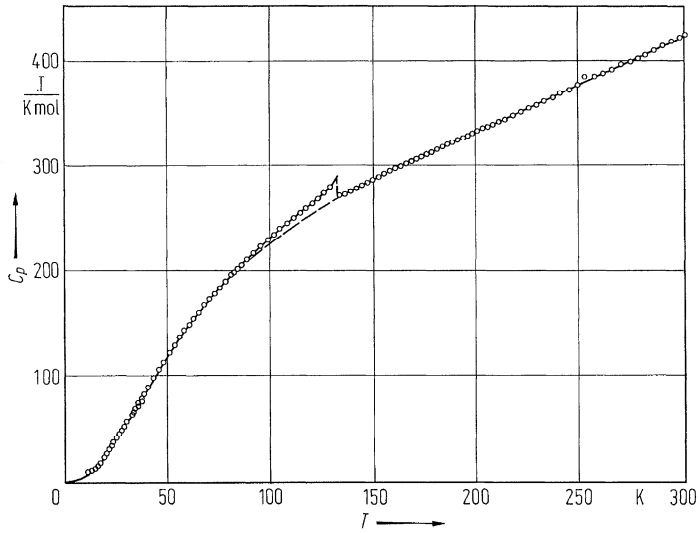

Fig. 64A-1-027. $(CH_3NHCH_2COOH)_3 \cdot CaCl_2$. C_p vs. T [79Mat]. C_p: molar heat capacity at constant pressure.

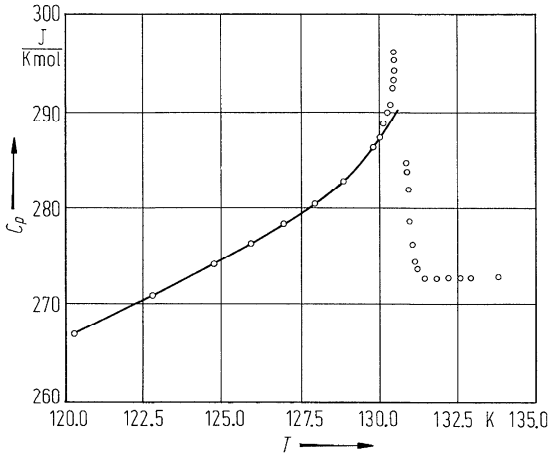

Fig. 64A-1-028. $(CH_3NHCH_2COOH)_3 \cdot CaCl_2$. C_p vs. T near Θ_f [84Tel]. The continuous line shows the specific heat by Landau prediction.

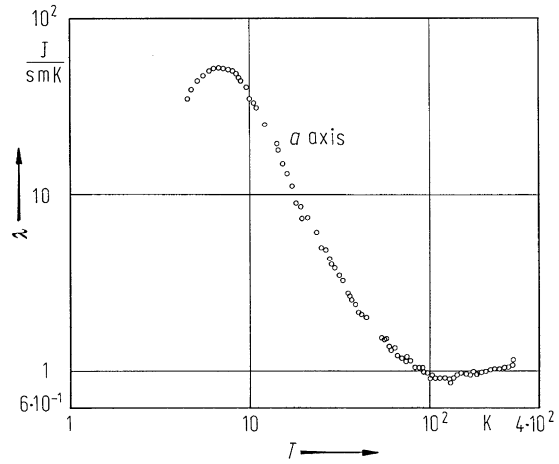

Fig. 64A-1-029. $(CH_3NHCH_2COOH)_3 \cdot CaCl_2$. λ vs. T [81Spo]. λ: thermal conductivity along the a axis.

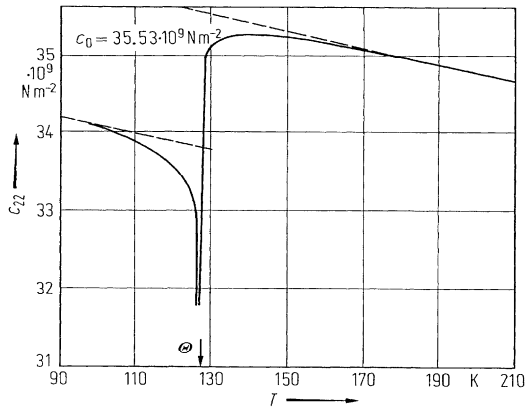

Fig. 64A-1-030. $(CH_3NHCH_2COOH)_3 \cdot CaCl_2$. c_{22} vs. T [78Sor]. c_{22}: elastic stiffness. c_0 shows the c_{22} value at Θ obtained by extrapolation of the curve shown by the dashed line.

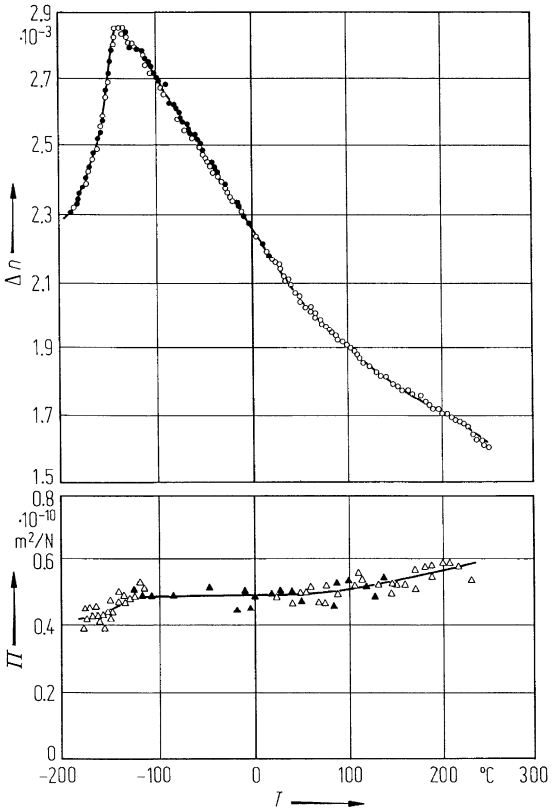

Fig. 64A-1-031. $(CH_3NHCH_2COOH)_3 \cdot CaCl_2$. Δn, Π vs. T [79Iva]. Δn: birefringence viewed along the Z axis, $\lambda = 550$ nm. Π: piezooptic constant for a compressive stress along the Y axis, $\lambda = 632.8$ nm. Data points marked by different symbols represent different runs in the experiment.

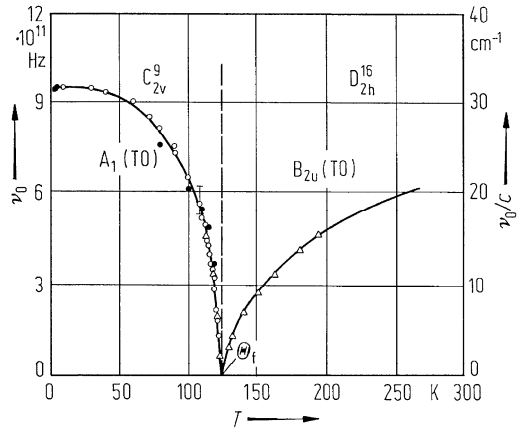

Fig. 64A-1-032. $(CH_3NHCH_2COOH)_3 \cdot CaCl_2$. ν_0 vs. T [83Koz]. ν_0: soft mode frequency. Triangles: measured by millimeter spectroscopy. Solid circles: data from far-infrared spectra [81Che]. Open circles: data from electric-field-induced Raman spectra [81Fel1].

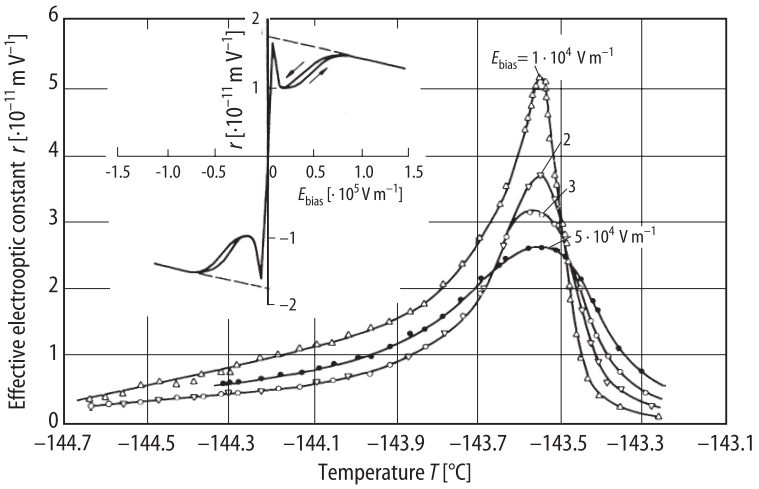

Fig. 64A-1-033. $(CH_3NHCH_2COOH)_3 \cdot CaCl_2$. r vs. T [79Iva]. r: effective electrooptic constant. Parameter: E_{bias}. $\lambda = 632.8$ nm.

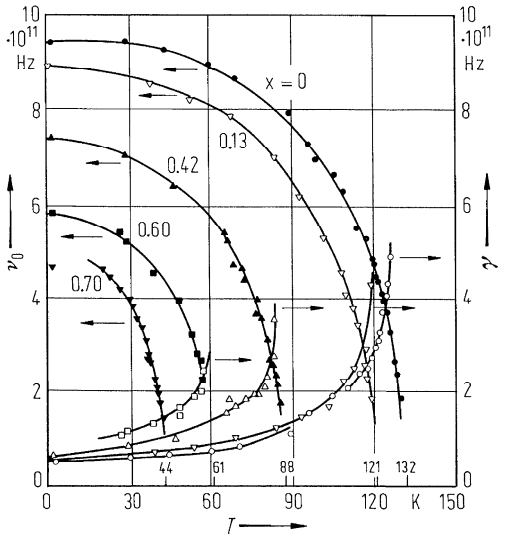

Fig. 64A-1-034. $(CH_3NHCH_2COOH)_3 \cdot CaCl_{2(1-x)}Br_{2x}$. ν_0 and γ vs. T [84Che]. Parameter: x, bromine concentration. ν_0: frequency of the lowest A_1(TO) mode, γ: damping of the mode, obtained from Raman spectrum. Scattering geometry is $X(YY)Z$. See also [81Fel2] and [84Sug].

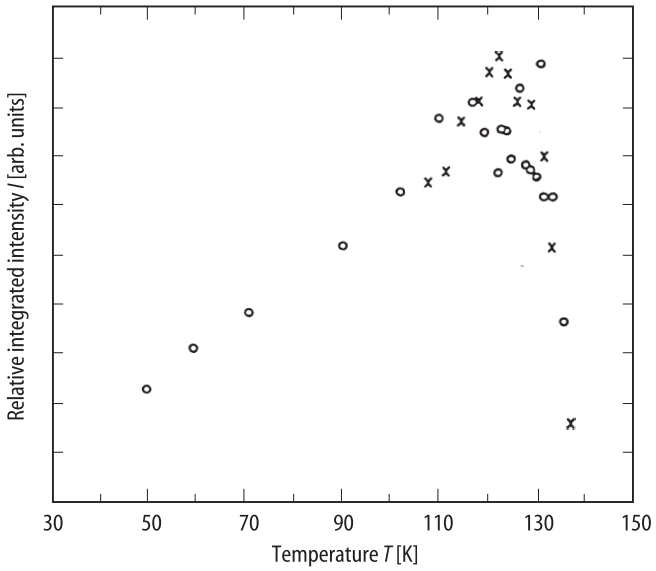

Fig. 64A-1-035. $(CH_3NHCH_2COOH)_3 \cdot CaCl_2$. I vs. T [90Che]. I: relative integrated intensity of Raman spectra. Cross: *XX*, circle: *YY*.

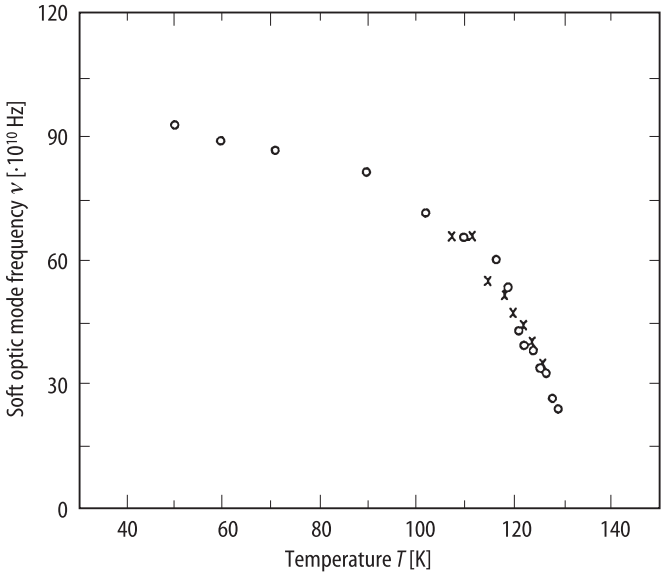

Fig. 64A-1-036. $(CH_3NHCH_2COOH)_3 \cdot CaCl_2$. ν vs. T [90Che]. ν: soft optic mode frequency. Cross: *XX*, circle: *YY*.

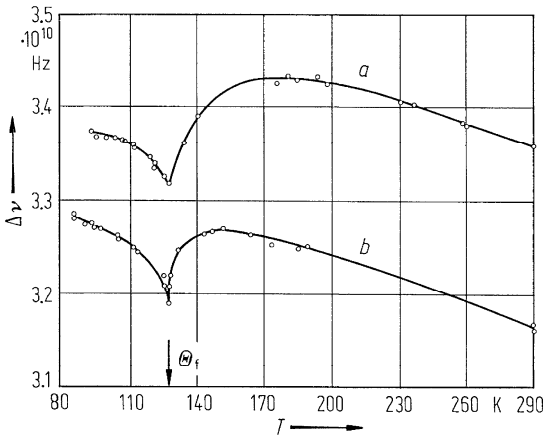

Fig. 64A-1-037. $(CH_3NHCH_2COOH)_3 \cdot CaCl_2$. $\Delta\nu$ vs. T [80Pro]. $\Delta\nu$: Brillouin scattering frequency shift ($\lambda = 488$ nm). Curve *a*: c_{22} mode, curve *b*: c_{11} mode.

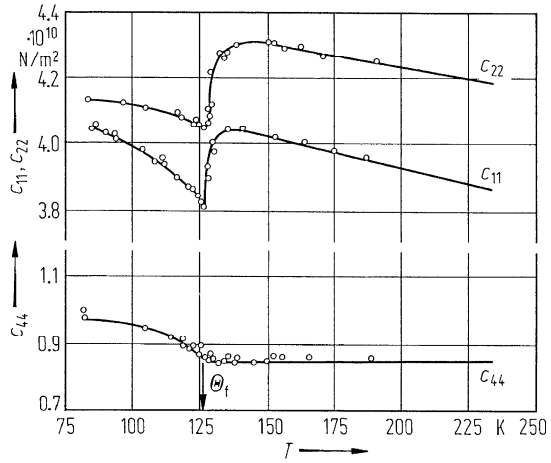

Fig. 64A-1-038. $(CH_3NHCH_2COOH)_3 \cdot CaCl_2$. c_{11}, c_{22}, c_{44} vs. T, obtained by Brillouin scattering [80Smo].

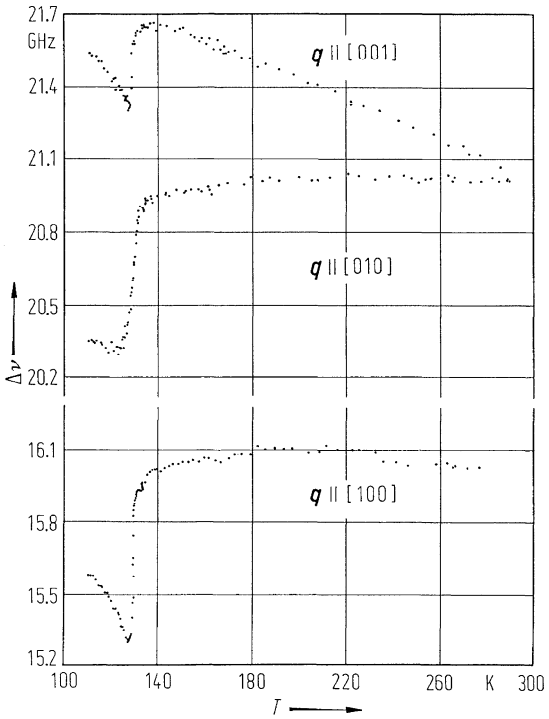

Fig. 64A-1-039. $(CH_3NHCH_2COOH)_3 \cdot CaCl_2$. $\Delta\nu$ vs. T [85Hik]. $\Delta\nu$: Brillouin scattering frequency shift of longitudinal acoustic waves propagating along the [100], [010] and [001] directions. $\lambda = 514.5$ nm, scattering angle: 90°.

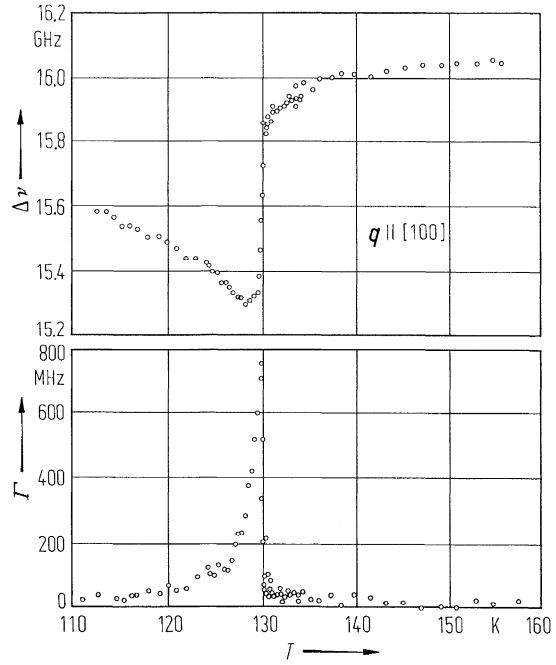

Fig. 64A-1-040. $(CH_3NHCH_2COOH)_3 \cdot CaCl_2$. $\Delta\nu$, Γ vs. T [85Hik]. $\Delta\nu$: Brillouin scattering frequency shift of a longitudinal wave propagating along the a axis. Γ: full width at half maximum. $\lambda = 514.5$ nm.

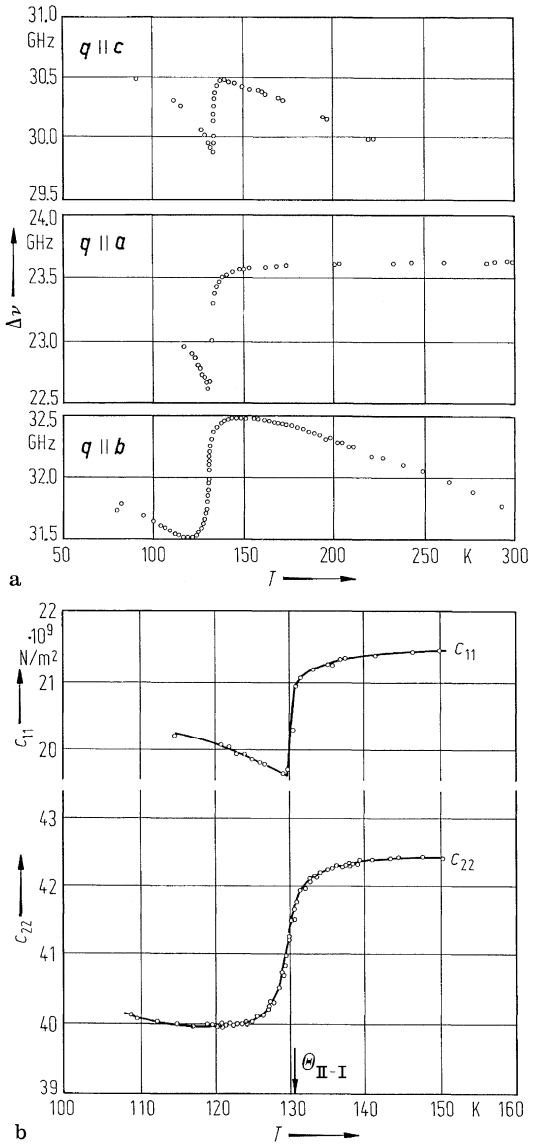

Fig. 64A-1-041. $(CH_3NHCH_2COOH)_3 \cdot CaCl_2$. $\Delta\nu$, c_{11}, c_{22} vs. T [85Smo]. Brillouin scattering with back scattering geometry. $\Delta\nu$: Brillouin frequency shift of phonon wave vector $\boldsymbol{q} \parallel \boldsymbol{a}$, $\boldsymbol{b}$ and $\boldsymbol{c}$ (**Fig. a**). c_{11}, c_{22}: elastic stiffnesses corresponding to the curves for $\boldsymbol{q} \parallel \boldsymbol{a}$ and $\boldsymbol{q} \parallel \boldsymbol{b}$ near Θ_{II-I} in Fig. a (**Fig. b**).

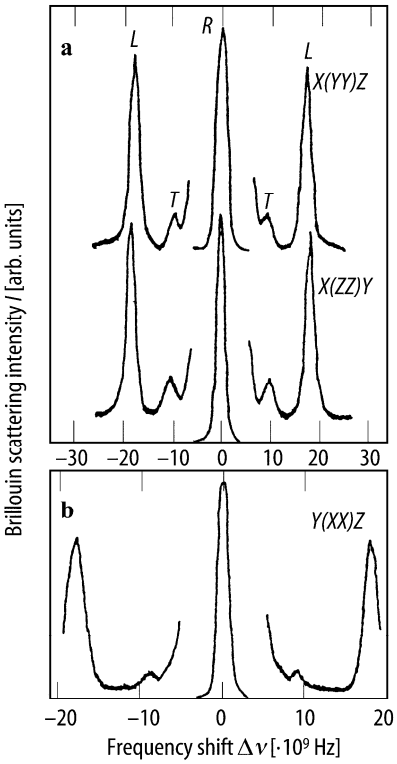

Fig. 64A-1-042. $(CH_3NHCH_2COOH)_3 \cdot CaCl_2$. I vs. $\Delta\nu$ [88Pri]. I: Brillouin scattering intensity. Parameter: scattering geometry. R: Rayleigh peak. L, T: longitudinal and transverse modes. (**a**) $X(YY)Z$, $X(ZZ)Y$; (**b**) $Y(XX)Z$.

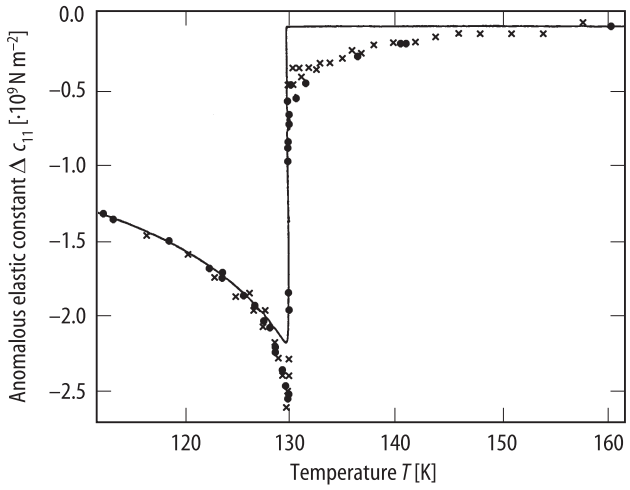

Fig. 64A-1-043. $(CH_3NHCH_2COOH)_3 \cdot CaCl_2$. Δc_{11} vs. T [89Che]. Δc_{11}: anomalous part of c_{11}. Solid line is the mean field prediction. Circle: $\theta = 23.78°$, cross: $\theta = 6.03°$.

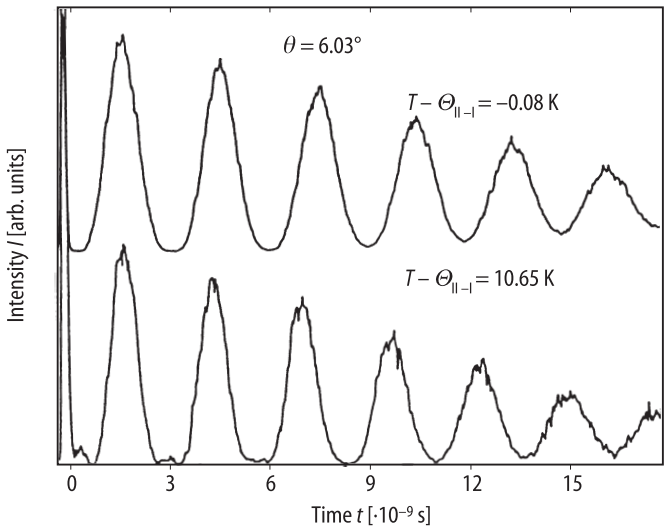

Fig. 64A-1-044. $(CH_3NHCH_2COOH)_3 \cdot CaCl_2$. *I* vs. *t* [89Che]. *I*: intensity of the induced Brillouin scattering. Parameter: $T - \Theta_{II–I}$.

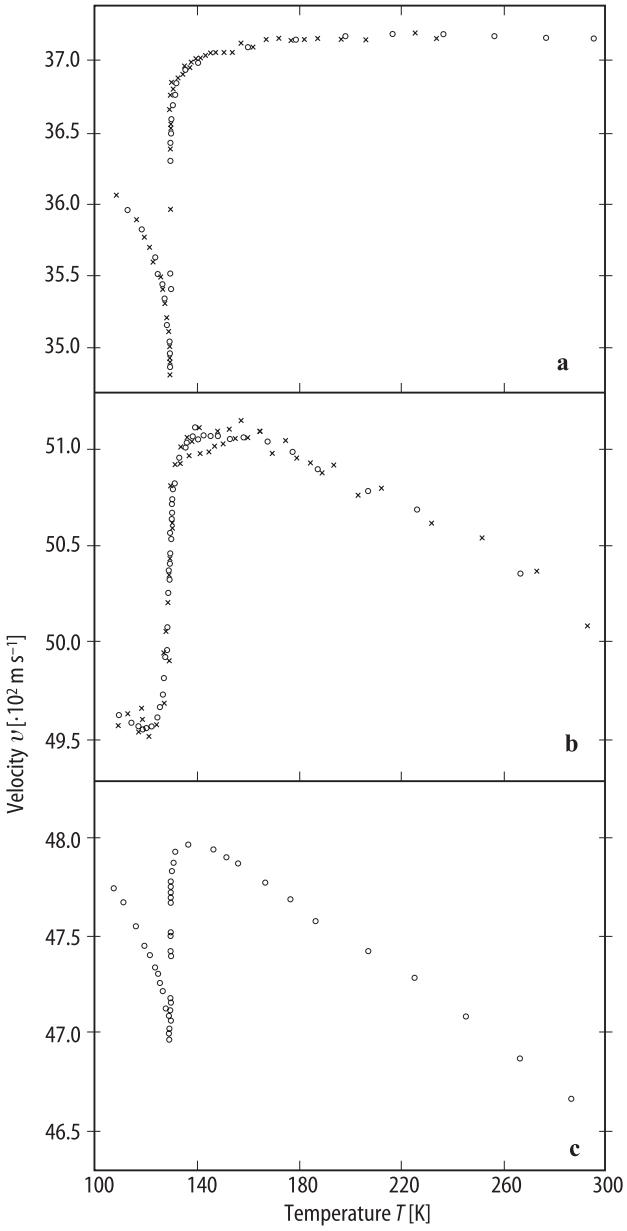

Fig. 64A-1-045. $(CH_3NHCH_2COOH)_3 \cdot CaCl_2$. v vs. T [89Che]. v: velocity of the LA mode measured by ISBS, (**a**) $\boldsymbol{q}$ || [100], (**b**) $\boldsymbol{q}$ || [010], (**c**) $\boldsymbol{q}$ || [001]. Circle: $\theta = 23.78°$, cross: $\theta = 6.03°$.

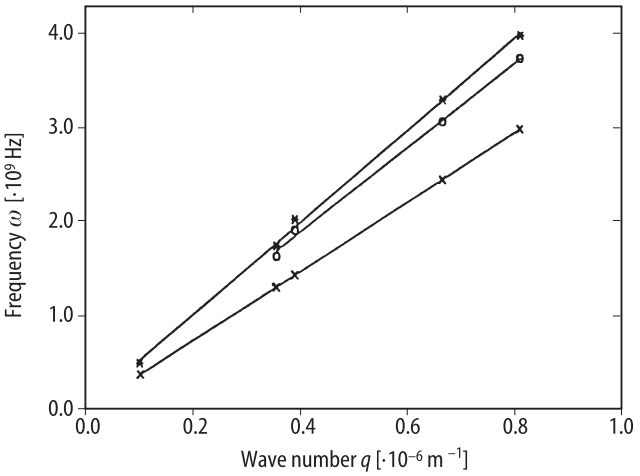

Fig. 64A-1-046. $(CH_3NHCH_2COOH)_3 \cdot CaCl_2$. ω vs. q [89Che]. T = RT. ω: frequency of the LA mode measured by ISBS for $\boldsymbol{q}$ || [100] (cross), $\boldsymbol{q}$ || [010] (asterisk) and $\boldsymbol{q}$ || [001] (circle).

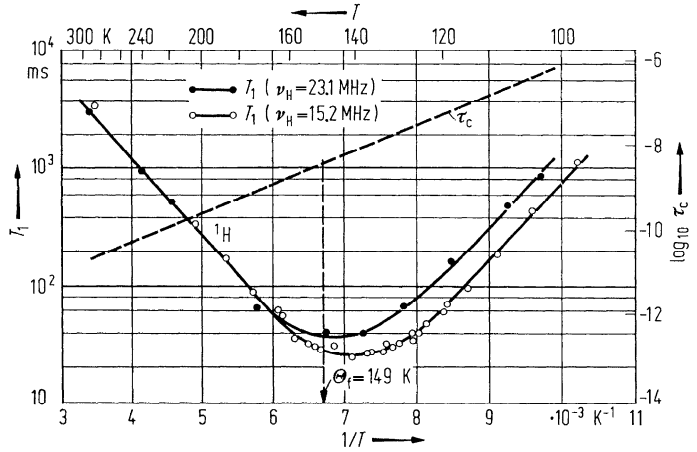

Fig. 64A-1-047. $(CH_3NHCH_2COOH)_3 \cdot CaCl_2$. T_1, $\log_{10}\tau_c$ vs. $1/T$ [70Bli]. T_1: proton spin-lattice relaxation time. τ_c: correlation time [s]. ν_H: Lamor frequency of proton.

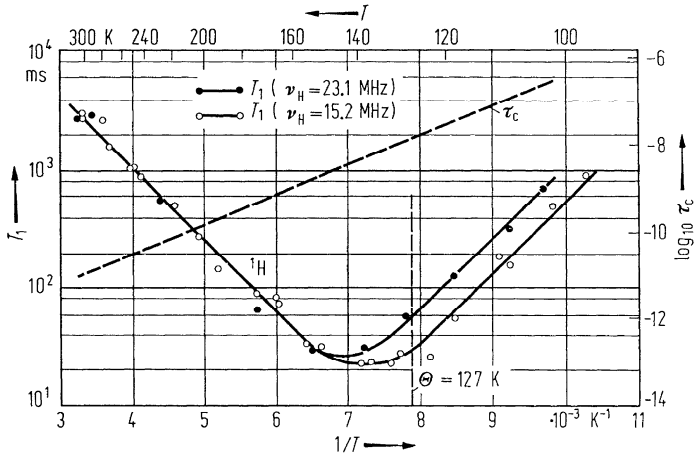

Fig. 64A-1-048. $(CH_3NDCH_2COOD)_3 \cdot CaCl_2$ (partially deuterated). T_1, $\log_{10}\tau_c$ vs. $1/T$ [70Bli]. T_1: proton spin-lattice relaxation time. τ_c: correlation time [s].

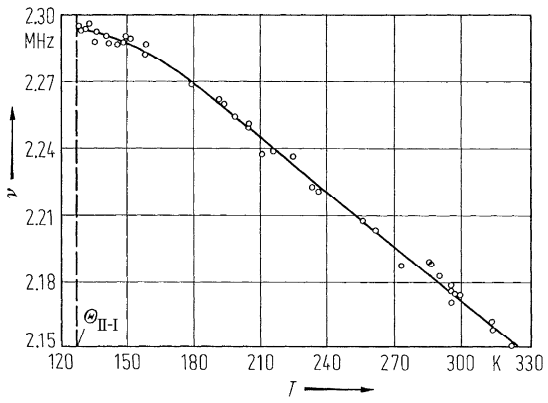

Fig. 64A-1-049. $(CH_3NHCH_2COOH)_3 \cdot CaCl_2$. ν vs. T [75Kad]. ν: ^{35}Cl quadrupole resonance frequency.

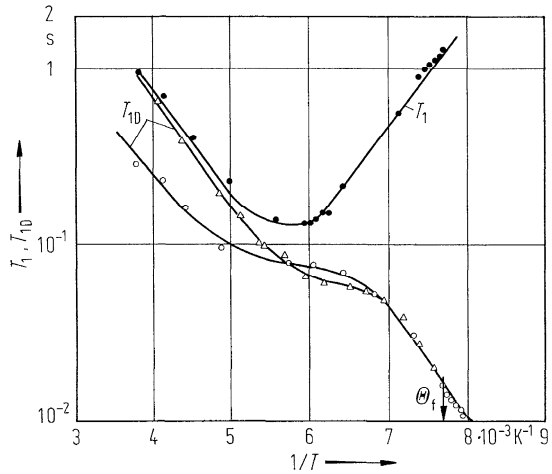

Fig. 64A-1-050. $(CH_3NHCH_2COOH)_3 \cdot CaCl_2$. T_1, T_{1D} vs. $1/T$ [84Eng]. T_1: proton spin-lattice relaxation time. T_{1D}: proton spin-lattice relaxation time in dipolar field. Open circle, full circle: ν_L = 90 MHz; triangle: ν_L = 60 MHz.

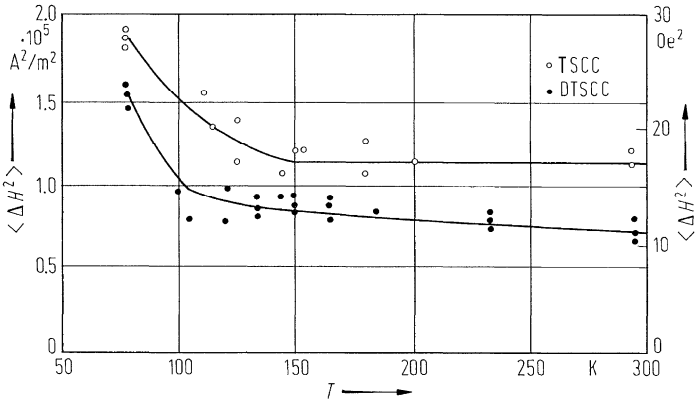

Fig. 64A-1-051. $(CH_3NHCH_2COOH)_3 \cdot CaCl_2$ (TSCC), deuterated TSCC (DTSCC). $\langle \Delta H^2 \rangle$ vs. T [84Eng]. $\langle \Delta H^2 \rangle$: proton NMR second moment for powder specimens.

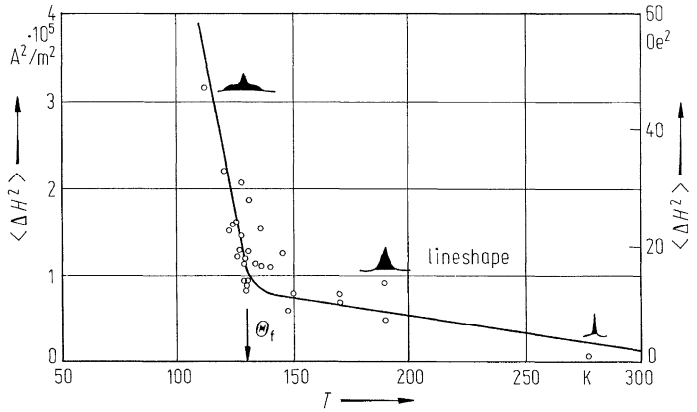

Fig. 64A-1-052. $(CH_3NHCH_2COOH)_3 \cdot CaCl_2$. $\langle \Delta H^2 \rangle$ vs. T [86Eng]. $\langle \Delta H^2 \rangle$: second moment of ^{15}N NMR resonance line. Powder 60 % enriched with ^{15}N nuclei.

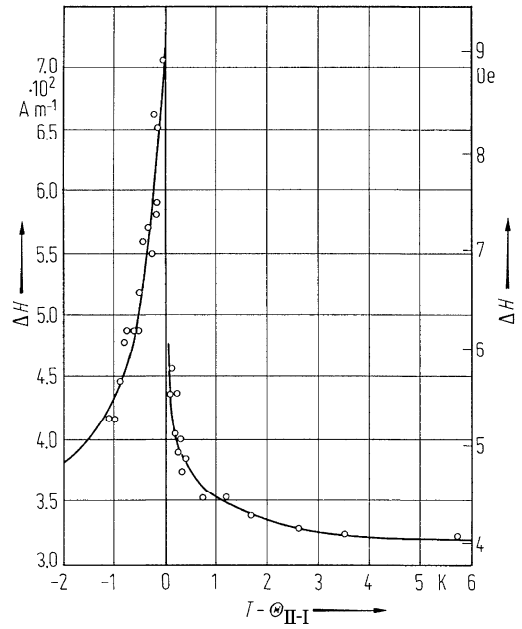

Fig. 64A-1-053. $(CH_3NHCH_2COOH)_3 \cdot CaCl_2$:$Mn^{2+}$. ΔH vs. $T - \Theta_{II-I}$ [76Lip]. ΔH: ESR line width of Mn^{2+}.

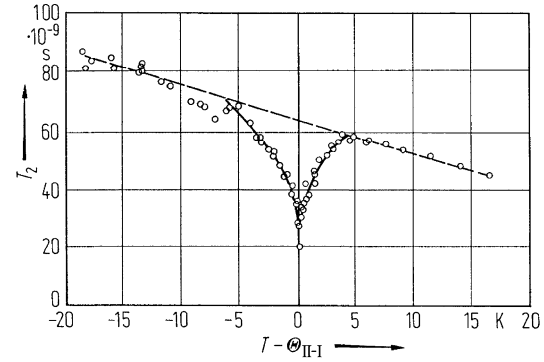

Fig. 64A-1-054. $(CH_3NHCH_2COOH)_3 \cdot CaCl_2$:$Mn^{2+}$. T_2 vs. $T - \Theta_{II-I}$ [76Win]. T_2: transverse relaxation time of Mn^{2+}.

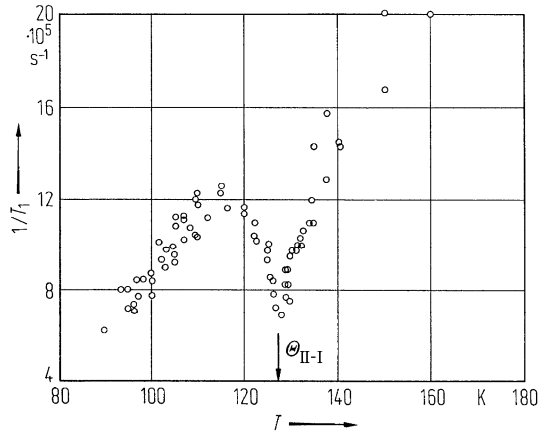

Fig. 64A-1-055. $(CH_3NHCH_2COOH)_3 \cdot CaCl_2:Mn^{2+}$. T_1^{-1} vs. T [78Bru]. T_1^{-1} : inverse of Mn^{2+} spin-lattice relaxation time.

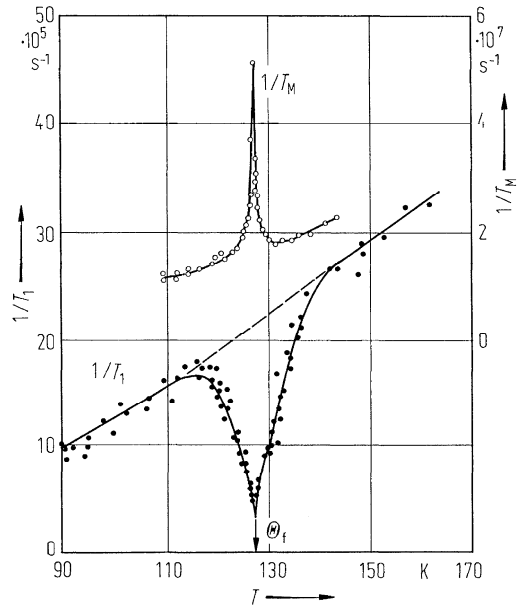

Fig. 64A-1-056. $(CH_3NHCH_2COOH)_3 \cdot CaCl_2:Mn^{2+}$. T_1^{-1}, T_M^{-1} vs. T [80Win]. T_1, T_M: longitudinal and transversal relaxation times of Mn^{2+}.

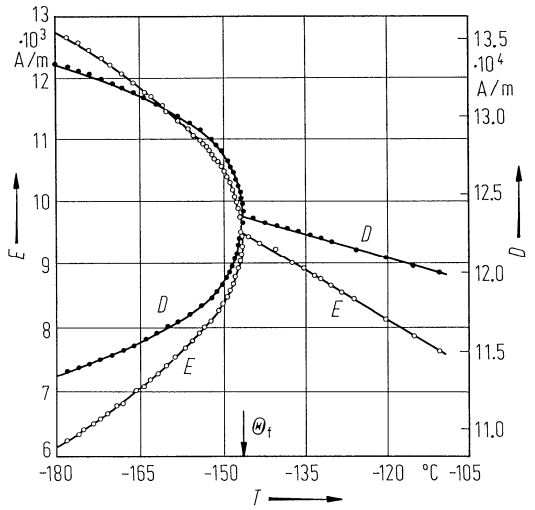

Fig. 64A-1-057. $(CH_3NHCH_2COOH)_3 \cdot CaCl_2$. *D*, *E* vs. *T* [81Kro]. *D*, *E*: spin Hamiltonian parameters for Fe^{3+} centers.

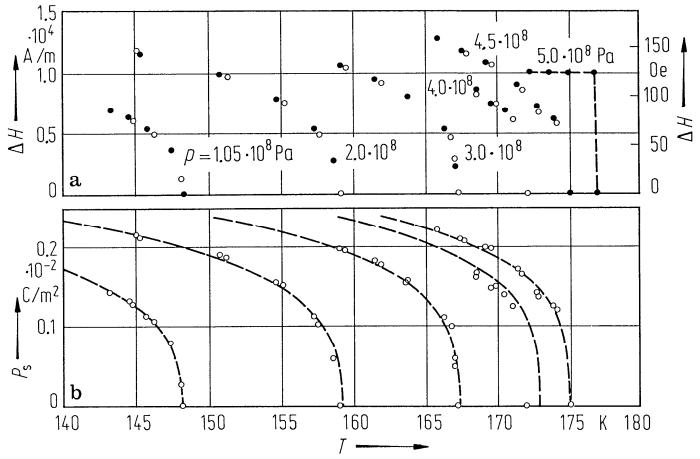

Fig. 64A-1-058. $(CH_3NHCH_2COOH)_3 \cdot CaCl_2:Mn^{2+}$. (**a**) ΔH vs. *T*, (**b**) P_s vs. *T* [81Rei]. ΔH: ESR line splitting of Mn^{2+} center. $M = -5/2 \leftrightarrow -3/2$, $m = -5/2$ (full circle), $m = -3/2$ (open circle). P_s: spontaneous polarization calculated from ΔH. Parameter: *p*.

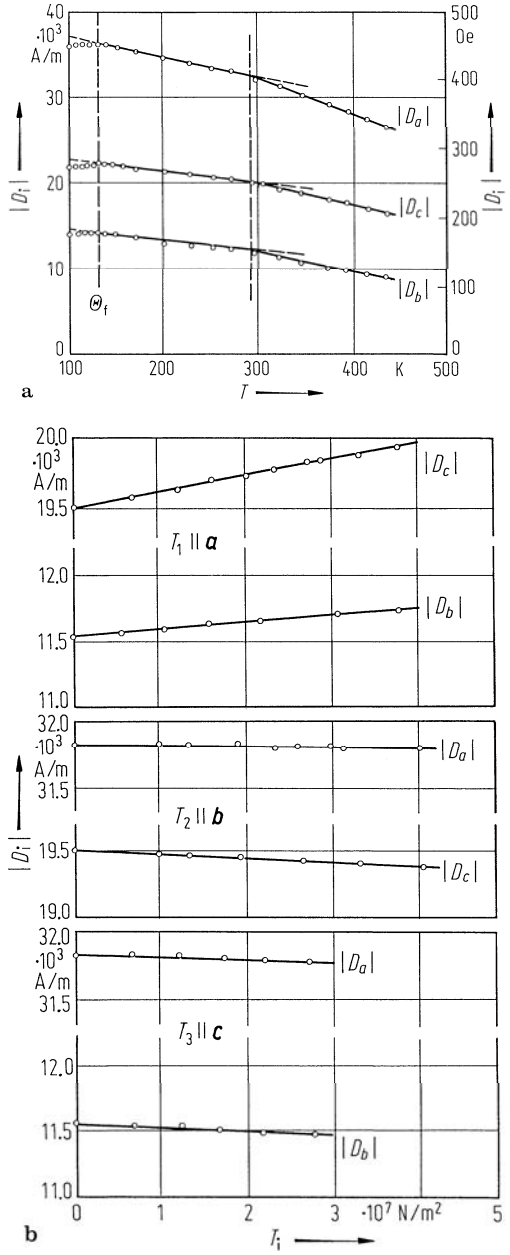

Fig. 64A-1-059. $(CH_3NHCH_2COOH)_3 \cdot CaCl_2:Mn^{2+}$. (**a**) $|D_i|$ vs. T, (**b**) $|D_i|$ vs. T_i [86Fuj]. D_i: spin Hamiltonian parameters for Mn^{2+} center. T_i: uniaxial stress. $T = 22.5$ °C.

References

62Pep Pepinsky, R., Makita, Y.: Bull. Am. Phys. Soc. [2] **7** (1962) 241.
65Mak Makita, Y.: J. Phys. Soc. Jpn. **20** (1965) 2073.
70Bli Blinc, R., Jamsek-Vilfan, M., Lahajnar, G., Hajdukovic, G.: J. Chem. Phys. **52** (1970) 6407.
72Ash Ashida, T., Bando, S., Kakudo, M.: Acta Crystallogr. Sect. B **28** (1972) 1560.
72Bar Bartuch, H., Windsch, W.: Phys. Status Solidi (a) **14** (1972) K51.
75Bli Blinc, R., Mali, M., Osredkar, R., Seliger, J.: J. Chem. Phys. **63** (1975) 35.
75Kad Kadaba, P.K., Pirnat, J., Trontelj, Z.: Chem. Phys. Lett. **32** (1975) 382.
75Nav Navalgund, R., Gupta, L.C.: J. Phys. Soc. Jpn. **39** (1975) 880.
75Win Windsch, W., Lippe, R., Völkel, G.: Solid State Commun. **17** (1975) 1375.
76Lip Lippe, R., Windsch, W., Völkel, G., Schulga, W.: Solid State Commun. **19** (1976) 587.
76Win Windsch, W.: Ferroelectrics **12** (1976) 63.
78Bru Brunner, W., Völkel, G., Windsch, W., Kurkin, I.N., Shlenkin, V.I.: Solid State Commun. **26** (1978) 853.
78Sat Sathyanarayan, S.G., Narayana, M., Sastry, G.S.: J. Chem. Phys. **68** (1978) 3122.
78Sor Sorge, G., Straube, U.: Ferroelectrics **21** (1978) 533.
79Iva Ivanov, N.R., Arndt, H.: Kristallografiya **24** (1979) 508; Sov. Phys. Crystallogr. (English Transl.) **24** (1979) 291.
79Mat Matsuo, T., Mansson, M., Sunner, S.: Acta Chem. Scand. A **33** (1979) 781.
80Pro Prokhorova, S.D., Smolensky, G.A., Siny, I.G., Kuzminov, E.G., Mikvabia, V.D., Arndt, H.: Ferroelectrics **25** (1980) 629.
80Smo Smolensky, G.A, Siny, I.G., Prokhorova, S.D., Kuzminov, E.G., Mikvabia, V.D.: J. Phys. Soc. Jpn. **49** (1980) Suppl. B **26**.
80Win Windsch, W., Völkel, G.: Ferroelectrics **24** (1980) 195.
81Che Chen, T., Schaack, G., Winterfeldt, V.: Ferroelectrics **39** (1981) 1131.
81Fel1 Feldkamp, G.E.: Ph. D. Thesis, University of Colorado (1981).
81Fel2 Feldkamp, G.E., Scott, J.F., Windsch, W.: Ferroelectrics **39** (1981) 1163.
81Kro Kröber, T., Wartewig, S., Windsch, W.: Phys. Status Solidi (b) **104** (1981) 177.
81Rei Reichelt, H., Windsch, W., Sienkiewicz, A.: Ferroelectrics **34** (1981) 195.
81Sor Sorge, G., Straube, U., Ivanov, N.R.: Phys. Status Solidi (a) **65** (1981) 189.
81Spo Spörl, G., Ullmann, S., Hässler, W., Hegenbarth, E., Malike, B.: Phys. Status Solidi (a) **63** (1981) K175.
81Vol Völkel, G., Windsch, W., Höselbarth, J., Brunner, W.: Ann. Phys., 7. Folge **38** (1981) 271.
83Deg Deguchi, K., Aramaki, N., Nakamura, E., Tanaka, K.: J. Phys. Soc. Jpn. **52** (1983) 1897.
83Fuj Fujimoto, M.: Ferroelectrics **47** (1983) 177.
83Koz Kozlov, G.V., Volkov, A.A., Scott, J.F., Feldkamp, G.E., Petzelt, J.: Phys. Rev. B **28** (1983) 255.
83Kuc Kuchler, J., Malige, B., Meister, R., Triebeneck, R., Windsch, W.: Cryst. Res. Technol. **18** (1983) 1325.
83Met Metz, H., Küchler, J., Böttcher, R., Windsch, W.: Chem. Phys. Lett. **97** (1983) 303.
84Che Chen, T., Schaack, G.: J. Phys. C **17** (1984) 3801.
84Eng Engelke, F., Michel, D., Pille, F.: Phys. Status Solidi (b) **125** (1984) 483.
84Fuj Fujimoto, S., Yasuda, N., Kawamura, A., Hachiga, T.: J. Phys. D **17** (1984) 1019.
84Mis Mishima, N., Itoh, K., Nakamura, E.: Acta Crystallogr. Sect. C **40** (1984) 1824.
84Sug Sugo, M., Kasahara, M., Tokunaga, M., Tatsuzaki, I.: J. Phys. Soc. Jpn. **53** (1984) 3234.
84Tel Tello, M.J., Pérez-Jubindo, M.A., López-Echarri, A., Socias, C.: Solid State Commun. **50** (1984) 957.
85Hik Hikita, T., Schnackenberg, P., Schmidt, V.H.: Phys. Rev. B **31** (1985) 299.
85Nak Nakamura, E., Itoh, K., Deguchi, K., Mishima, N.: Jpn. J. Appl. Phys. **24** (1985) Suppl. 24–2, 393.
85Rot Roth, R., Schaack, G., Hochheimer, H. D.: Solid State Commun. **55** (1985) 121.
85Saw Sawada, A., Horioka, M.: Jpn. J. Appl. Phys. **24** (1985) Suppl. 24–2, 390.
85Smo Smolensky, G.A., Siny, I.G., Tagantsev, A.K., Prokhorova, S.D., Windsch, W.: Ferroelectrics **64** (1985) 221.
86Eng Engelke, F., Michel, D., Windsch, W., Petersson, J.: Phys. Status Solidi (b) **134** (1986) 29.

86Fuj Fujimoto, M., Jerza, K.S.: Philos. Mag. B **53** (1986) 521.
86Paw Pawlaczyk, Cz., Unruh, H.-G., Petzelt, J.: Phys. Status Solidi (b) **136** (1986) 435.
88Pri Prieto, C., Ramirez, R., Gonzalo, J.A., Windsch, W.: Phys. Status Solidi (a) **108** (1988) K9.
89Che Chen, L.-T., Nelson, K.A.: Phys. Rev. B **39** (1989) 9437.
90Che Chen, T., Scott, J.F.: J. Raman Spectrosc. **21** (1990) 761.
92Hik Hikita, T., Maruyama, T.: J. Phys. Soc. Jpn. **61** (1992) 2840.

No. 64A-2 $(CH_3NHCH_2COOH)_3 \cdot CaBr_2$, Tris-sarcosine calcium bromide (TSCB)

(M = 467.17)

1a	Ferroelectricity in pressure-induced phase was reported by Fujimoto et al. in 1982.	82Fuj
2a	Crystal growth: evaporation or cooling method from aqueous solution	82Fuj
5a	Dielectric constant: Fig. 64A-2-001, Fig. 64A-2-002. Curie-Weiss constant: Fig. 64A-2-003. Phase diagram with regard to p: Fig. 64A-2-004.	
c	Spontaneous polarization: Fig. 64A-2-005.	
13b	ESR of Mn^{2+} doped crystal: see Table 64A-1-010 in No. 64A-1.	

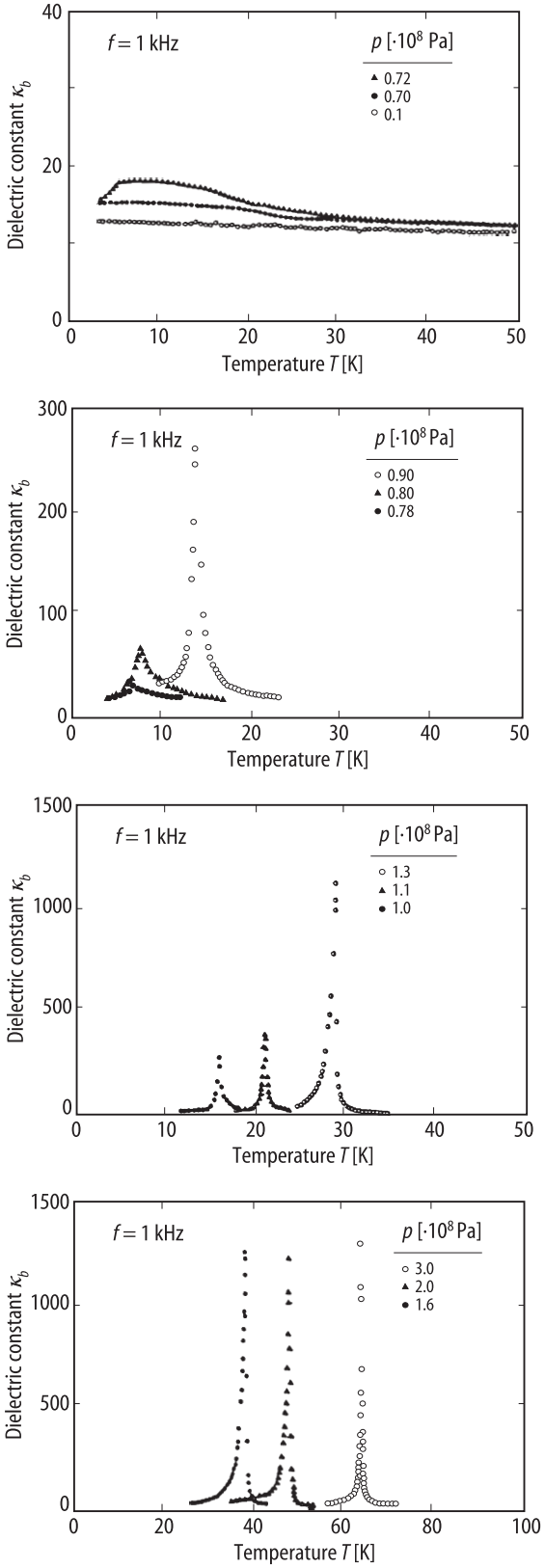

Fig. 64A-2-001. $(CH_3NHCH_2COOH)_3 \cdot CaBr_2$ (TSCB). κ_b vs. T [92Hik]. Parameter: p.

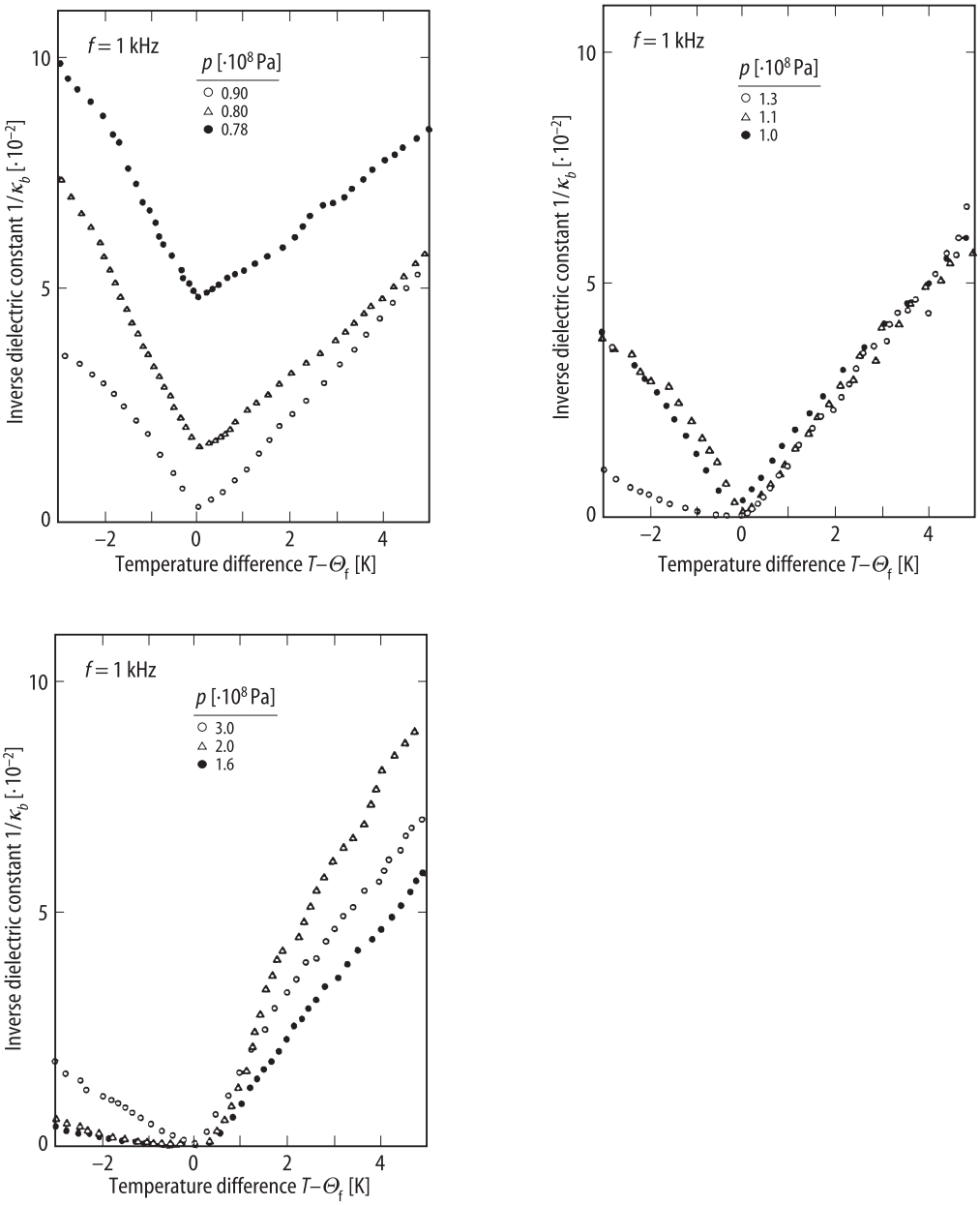

Fig. 64A-2-002. $(CH_3NHCH_2COOH)_3 \cdot CaBr_2$ (TSCB). $1/\kappa_b$ vs. $T - \Theta_f$ [92Hik]. Parameter: p.

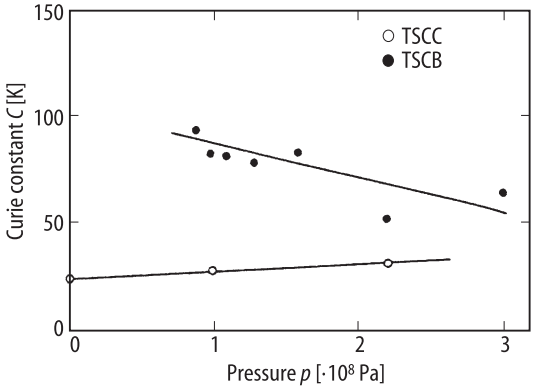

Fig. 64A-2-003. $(CH_3NHCH_2COOH)_3 \cdot CaBr_2$ (TSCB), $(CH_3NHCH_2COOH)_3 \cdot CaCl_2$ (TSCC). C vs. p [92Hik]. C: Curie-Weiss constant at $f = 1$ kHz.

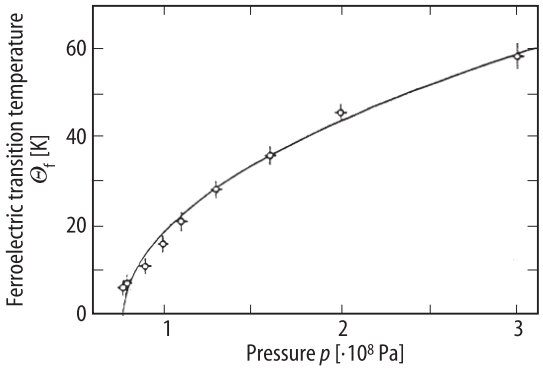

Fig. 64A-2-004. $(CH_3NHCH_2COOH)_3 \cdot CaBr_2$ (TSCB). Θ_f vs. p [92Hik].

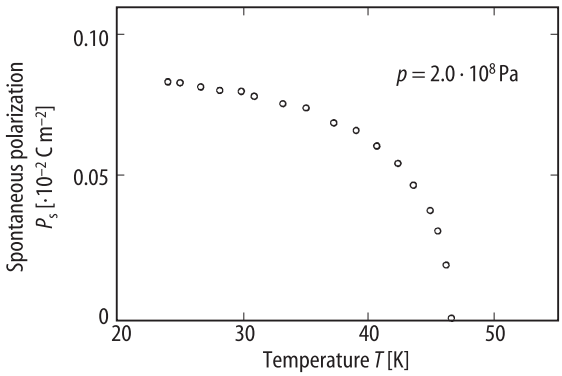

Fig. 64A-2-005. $(CH_3NHCH_2COOH)_3 \cdot CaBr_2$ (TSCB). P_s vs. T at $p = 2.0 \cdot 10^8$ Pa [92Hik].

References

82Fuj Fujimoto, S., Yasuda, N., Kashiki, H.: J. Phys. D **15** (1982) 487.
92Hik Hikita, T., Maruyama, T.: J. Phys. Soc. Jpn. **61** (1992) 2840.